Measurement of high-Q^2 neutral current deep inelastic $e^+ p$ scattering cross sections with a longitudinally polarized positron beam at HERA

H. Abramowicz,[45,aa] I. Abt,[35] L. Adamczyk,[13] M. Adamus,[54] R. Aggarwal,[7] S. Antonelli,[4] P. Antonioli,[3] A. Antonov,[33] M. Arneodo,[50] O. Arslan,[5] V. Aushev,[26,27] Y. Aushev,[27,w] O. Bachynska,[15] A. Bamberger,[19] A. N. Barakbaev,[25] G. Barbagli,[17] G. Bari,[3] F. Barreiro,[30] N. Bartosik,[15] D. Bartsch,[5] M. Basile,[4] O. Behnke,[15] J. Behr,[15] U. Behrens,[15] L. Bellagamba,[3] A. Bertolin,[39] S. Bhadra,[57] M. Bindi,[4] C. Blohm,[15] V. Bokhonov,[26] T. Bołd,[13] K. Bondarenko,[27] E. G. Boos,[25] K. Borras,[15] D. Boscherini,[3] D. Bot,[15] I. Brock,[5] E. Brownson,[56] R. Brugnera,[40] N. Brümmer,[37] A. Bruni,[3] G. Bruni,[3] B. Brzozowska,[53] P. J. Bussey,[20] B. Bylsma,[37] A. Caldwell,[35] M. Capua,[8] R. Carlin,[40] C. D. Catterall,[57] S. Chekanov,[1] J. Chwastowski,[12,d] J. Ciborowski,[53,ee] R. Ciesielski,[15,e] L. Cifarelli,[4] F. Cindolo,[3] A. Contin,[4] A. M. Cooper-Sarkar,[38] N. Coppola,[15,f] M. Corradi,[3] F. Corriveau,[31] M. Costa,[49] G. D'Agostini,[43] F. Dal Corso,[39] J. del Peso,[30] R. K. Dementiev,[34] S. De Pasquale,[4,a] M. Derrick,[1] R. C. E. Devenish,[38] D. Dobur,[19,p] B. A. Dolgoshein,[33,v] G. Dolinska,[27] A. T. Doyle,[20] V. Drugakov,[16] L. S. Durkin,[37] S. Dusini,[39] Y. Eisenberg,[55] P. F. Ermolov,[34,v] A. Eskreys,[12,v] S. Fang,[15,g] S. Fazio,[8] J. Ferrando,[20] M. I. Ferrero,[49] J. Figiel,[12] B. Foster,[38,y] G. Gach,[13] A. Galas,[12] E. Gallo,[17] A. Garfagnini,[40] A. Geiser,[15] I. Gialas,[21,s] A. Gizhko,[27,x] L. K. Gladilin,[34] D. Gladkov,[33] C. Glasman,[30] O. Gogota,[27] Yu. A. Golubkov,[34] P. Göttlicher,[15,h] I. Grabowska-Bołd,[13] J. Grebenyuk,[15] I. Gregor,[15] G. Grigorescu,[36] G. Grzelak,[53] O. Gueta,[45] M. Guzik,[13] C. Gwenlan,[38] T. Haas,[15] W. Hain,[15] R. Hamatsu,[48] J. C. Hart,[44] H. Hartmann,[5] G. Hartner,[57] E. Hilger,[5] D. Hochman,[55] R. Hori,[47] A. Hüttmann,[15] Z. A. Ibrahim,[10] Y. Iga,[42] R. Ingbir,[45] M. Ishitsuka,[46] H. -P. Jakob,[5] F. Januschek,[15] T. W. Jones,[52] M. Jüngst,[5] I. Kadenko,[27] B. Kahle,[15] S. Kananov,[45] T. Kanno,[46] U. Karshon,[55] F. Karstens,[19,q] I. I. Katkov,[15,i] M. Kaur,[7] P. Kaur,[7] A. Keramidas,[36] L. A. Khein,[34] J. Y. Kim,[9] D. Kisielewska,[13] S. Kitamura,[48,cc] R. Klanner,[22] U. Klein,[15,j] E. Koffeman,[36] N. Kondrashova,[27,x] O. Kononenko,[27] P. Kooijman,[36] Ie. Korol,[27] I. A. Korzhavina,[34] A. Kotański,[14] U. Kötz,[15] H. Kowalski,[15] O. Kuprash,[15] M. Kuze,[46] A. Lee,[37] B. B. Levchenko,[34] A. Levy,[45] V. Libov,[15] S. Limentani,[40] T. Y. Ling,[37] M. Lisovyi,[15] E. Lobodzinska,[15] W. Lohmann,[16] B. Löhr,[15] E. Lohrmann,[22] K. R. Long,[23] A. Longhin,[39,z] D. Lontkovskyi,[15] O. Yu. Lukina,[34] J. Maeda,[46,bb] S. Magill,[1] I. Makarenko,[15] J. Malka,[15] R. Mankel,[15] A. Margotti,[3] G. Marini,[43] J. F. Martin,[51] A. Mastroberardino,[8] M. C. K. Mattingly,[2] I. -A. Melzer-Pellmann,[15] S. Mergelmeyer,[5] S. Miglioranzi,[15,k] F. Mohamad Idris,[10] V. Monaco,[49] A. Montanari,[15] J. D. Morris,[6,b] K. Mujkic,[15,l] B. Musgrave,[1] K. Nagano,[24] T. Namsoo,[15,m] R. Nania,[3] A. Nigro,[43] Y. Ning,[11] T. Nobe,[46] D. Notz,[15] R. J. Nowak,[53] A. E. Nuncio-Quiroz,[5] B. Y. Oh,[41] N. Okazaki,[47] K. Olkiewicz,[12] Yu. Onishchuk,[27] K. Papageorgiu,[21] A. Parenti,[15] E. Paul,[5] J. M. Pawlak,[53] B. Pawlik,[12] P. G. Pelfer,[18] A. Pellegrino,[36] W. Perlański,[53,ff] H. Perrey,[15] K. Piotrzkowski,[29] P. Pluciński,[54,gg] N. S. Pokrovskiy,[25] A. Polini,[3] A. S. Proskuryakov,[34] M. Przybycień,[13] A. Raval,[15] D. D. Reeder,[56] B. Reisert,[35] Z. Ren,[11] J. Repond,[1] Y. D. Ri,[48,dd] A. Robertson,[38] P. Roloff,[15,k] I. Rubinsky,[15] M. Ruspa,[50] R. Sacchi,[49] U. Samson,[5] G. Sartorelli,[4] A. A. Savin,[56] D. H. Saxon,[20] M. Schioppa,[8] S. Schlenstedt,[16] P. Schleper,[22] W. B. Schmidke,[35] U. Schneekloth,[15] V. Schönberg,[5] T. Schörner-Sadenius,[15] J. Schwartz,[31] F. Sciulli,[11] L. M. Shcheglova,[34] R. Shehzadi,[5] S. Shimizu,[47,k] I. Singh,[7] I. O. Skillicorn,[20] W. Słomiński,[14] W. H. Smith,[56] V. Sola,[22] A. Solano,[49] D. Son,[28] V. Sosnovtsev,[33] A. Spiridonov,[15,n] H. Stadie,[22] L. Stanco,[39] N. Stefaniuk,[27] A. Stern,[45] T. P. Stewart,[51] A. Stifutkin,[33] P. Stopa,[12] S. Suchkov,[33] G. Susinno,[8] L. Suszycki,[13] J. Sztuk-Dambietz,[22] D. Szuba,[22] J. Szuba,[15,o] A. D. Tapper,[23] E. Tassi,[8,c] J. Terrón,[30] T. Theedt,[15] H. Tiecke,[36] K. Tokushuku,[24,t] J. Tomaszewska,[15] V. Trusov,[27] T. Tsurugai,[32] M. Turcato,[22] O. Turkot,[27,x] T. Tymieniecka,[54,hh] M. Vázquez,[36,k] A. Verbytskyi,[15] O. Viazlo,[27] N. N. Vlasov,[19,r] R. Walczak,[38] W. A. T. Wan Abdullah,[10] J. J. Whitmore,[41] K. Wichmann,[15] L. Wiggers,[36] M. Wing,[52] M. Wlasenko,[5] G. Wolf,[15] H. Wolfe,[56] K. Wrona,[15] A. G. Yagües-Molina,[15] S. Yamada,[24] Y. Yamazaki,[24,u] R. Yoshida,[1] C. Youngman,[15] O. Zabiegalov,[27,x] A. F. Żarnecki,[53] L. Zawiejski,[12] O. Zenaiev,[15] W. Zeuner,[15,k] B. O. Zhautykov,[25] N. Zhmak,[26] A. Zichichi,[4] Z. Zolkapli,[10] and D. S. Zotkin[34]

(ZEUS Collaboration)

[1]*Argonne National Laboratory, Argonne, Illinois 60439-4815, USA*
[2]*Andrews University, Berrien Springs, Michigan 49104-0380, USA*
[3]*INFN Bologna, Bologna, Italy*
[4]*University and INFN Bologna, Bologna, Italy*
[5]*Physikalisches Institut der Universität Bonn, Bonn, Germany*
[6]*H.H. Wills Physics Laboratory, University of Bristol, Bristol, United Kingdom*
[7]*Department of Physics, Panjab University, Chandigarh, India*

[8]*Physics Department and INFN, Calabria University, Cosenza, Italy*
[9]*Institute for Universe and Elementary Particles, Chonnam National University, Kwangju, South Korea*
[10]*Jabatan Fizik, Universiti Malaya, 50603 Kuala Lumpur, Malaysia*
[11]*Nevis Laboratories, Columbia University, Irvington on Hudson, New York 10027, USA*
[12]*The Henryk Niewodniczanski Institute of Nuclear Physics, Polish Academy of Sciences, Krakow, Poland*
[13]*Faculty of Physics and Applied Computer Science, AGH-University of Science and Technology, Krakow, Poland*
[14]*Department of Physics, Jagellonian University, Cracow, Poland*
[15]*Deutsches Elektronen-Synchrotron DESY, Hamburg, Germany*
[16]*Deutsches Elektronen-Synchrotron DESY, Zeuthen, Germany*
[17]*INFN Florence, Florence, Italy*
[18]*University and INFN Florence, Florence, Italy*
[19]*Fakultät für Physik der Universität Freiburg i.Br., Freiburg im Breisgau, Germany*
[20]*School of Physics and Astronomy, University of Glasgow, Glasgow, United Kingdom*
[21]*Department of Engineering in Management and Finance, University of the Aegean, Chios, Greece*
[22]*Institute of Experimental Physics, Hamburg University, Hamburg, Germany*
[23]*High Energy Nuclear Physics Group, Imperial College London, London, United Kingdom*
[24]*Institute of Particle and Nuclear Studies, KEK, Tsukuba, Japan*
[25]*Institute of Physics and Technology of Ministry of Education and Science of Kazakhstan, Almaty, Kazakhstan*
[26]*Institute for Nuclear Research, National Academy of Sciences, Kyiv, Ukraine*
[27]*Department of Nuclear Physics, National Taras Shevchenko University of Kyiv, Kyiv, Ukraine*
[28]*Center for High Energy Physics, Kyungpook National University, Daegu, South Korea*
[29]*Institut de Physique Nucléaire, Université Catholique de Louvain, Louvain-la-Neuve, Belgium*

[a]Present address: University of Salerno, Italy.
[b]Present address: Queen Mary University of London, United Kingdom.
[c]Also at Institute of Experimental Physics, Hamburg University, Hamburg, Germany.
[d]Also at Faculty of Physics, Mathemathics and Applied Computer Science, Cracow University of Technology, Poland.
[e]Present address: Rockefeller University, New York, New York 10065, USA.
[f]Now at DESY Group FS-CFEL-1.
[g]Present address: Institute of High Energy Physics, Beijing, China.
[h]Present address: DESY Group FEB, Hamburg, Germany.
[i]Also at Moscow State University, Russia.
[j]Present address: University of Liverpool, United Kingdom.
[k]Present address: CERN, Geneva, Switzerland.
[l]Also at University College London, United Kingdom.
[m]Present address: Goldman Sachs, London, United Kingdom.
[n]Also at Institute of Theoretical and Experimental Physics, Moscow, Russia.
[o]Also at FPACS, AGH-UST, Cracow, Poland.
[p]Present address: Istituto Nucleare di Fisica Nazionale (INFN), Pisa, Italy.
[q]Present address: Haase Energie Technik AG, Neumünster, Germany.
[r]Present address: Department of Physics, University of Bonn, Germany.
[s]Also at DESY, Germany.
[t]Also at University of Tokyo, Japan.
[u]Present address: Kobe University, Japan.
[v]Deceased.
[w]Also member of Kyiv Polytechnic Institute, National Technical University of Ukraine, Kyiv, Ukraine.
[x]Also member of National University of Kyiv - Mohyla Academy, Kyiv, Ukraine.
[y]Alexander von Humboldt Professor; also at DESY and University of Oxford.
[z]Present address: LNF, Frascati, Italy.
[aa]Also at Max Planck Institute for Physics, Munich, Germany, External Scientific Member.
[bb]Present address: Tokyo Metropolitan University, Japan.
[cc]Present address: Nihon Institute of Medical Science, Japan.
[dd]Present address: Osaka University, Osaka, Japan.
[ee]Also at Łódź University, Poland.
[ff]Also member of Łódź University, Poland.
[gg]Present address: Department of Physics, Stockholm University, Stockholm, Sweden.
[hh]Also at Cardinal Stefan Wyszyński University, Warsaw, Poland.

[30]*Departamento de Física Teórica, Universidad Autónoma de Madrid, Madrid, Spain*
[31]*Department of Physics, McGill University, Montréal, Québec H3A 2T8, Canada*
[32]*Faculty of General Education, Meiji Gakuin University, Yokohama, Japan*
[33]*Moscow Engineering Physics Institute, Moscow, Russia*
[34]*Skobeltsyn Institute of Nuclear Physics, Lomonosov Moscow State University, Moscow, Russia*
[35]*Max-Planck-Institut für Physik, München, Germany*
[36]*NIKHEF and University of Amsterdam, Amsterdam, The Netherlands*
[37]*Physics Department, Ohio State University, Columbus, Ohio 43210, USA*
[38]*Department of Physics, University of Oxford, Oxford, United Kingdom*
[39]*INFN Padova, Padova, Italy*
[40]*Dipartimento di Fisica dell' Università and INFN, Padova, Italy*
[41]*Department of Physics, Pennsylvania State University, University Park, Pennsylvania 16802, USA*
[42]*Polytechnic University, Tokyo, Japan*
[43]*Dipartimento di Fisica, Università La Sapienzaand INFN, Rome, Italy*
[44]*Rutherford Appleton Laboratory, Chilton, Didcot, Oxon, United Kingdom*
[45]*Raymond and Beverly Sackler Faculty of Exact Sciences, School of Physics, Tel Aviv University, Tel Aviv, Israel*
[46]*Department of Physics, Tokyo Institute of Technology, Tokyo, Japan*
[47]*Department of Physics, University of Tokyo, Tokyo, Japan*
[48]*Department of Physics, Tokyo Metropolitan University, Tokyo, Japan*
[49]*Università di Torino and INFN, Torino, Italy*
[50]*Università del Piemonte Orientale, Novara, and INFN, Torino, Italy*
[51]*Department of Physics, University of Toronto, Toronto, Ontario M5S 1A7, Canada*
[52]*Physics and Astronomy Department, University College London, London, United Kingdom*
[53]*Faculty of Physics, University of Warsaw, Warsaw, Poland*
[54]*National Centre for Nuclear Research, Warsaw, Poland*
[55]*Department of Particle Physics and Astrophysics, Weizmann Institute, Rehovot, Israel*
[56]*Department of Physics, University of Wisconsin, Madison, Wisconsin 53706, USA*
[57]*Department of Physics, York University, Ontario M3J 1P3, Canada*
(Received 10 December 2012; published 20 March 2013)

Measurements of neutral current cross sections for deep inelastic scattering in e^+p collisions at HERA with a longitudinally polarized positron beam are presented. The single-differential cross-sections $d\sigma/dQ^2$, $d\sigma/dx$ and $d\sigma/dy$ and the reduced cross section $\tilde{\sigma}$ are measured in the kinematic region $Q^2 > 185$ GeV^2 and $y < 0.9$, where Q^2 is the four-momentum transfer squared, x the Bjorken scaling variable and y the inelasticity of the interaction. The measurements are performed separately for positively and negatively polarized positron beams. The measurements are based on an integrated luminosity of 135.5 pb^{-1} collected with the ZEUS detector in 2006 and 2007 at a center-of-mass energy of 318 GeV. The structure functions $\tilde{F}_3$ and $F_3^{\gamma Z}$ are determined by combining the e^+p results presented in this paper with previously published e^-p neutral current results. The asymmetry parameter A^+ is used to demonstrate the parity violation predicted in electroweak interactions. The measurements are well described by the predictions of the Standard Model.

DOI: 10.1103/PhysRevD.87.052014 PACS numbers: 12.38.−t, 13.85.Qk

I. INTRODUCTION

The study of deep inelastic scattering (DIS) of leptons off nucleons has contributed significantly to tests of the Standard Model (SM) of the electroweak and strong interactions. The structure of nucleons has mainly been determined from DIS experiments. The ep collider HERA has allowed an extension in the four-momentum-transfer squared, Q^2, and in Bjorken x by several orders of magnitude with respect to previous fixed-target experiments [1]. The higher Q^2 reach of HERA has also allowed the exploration of the electroweak sector of the SM.

The ZEUS and H1 Collaborations have both measured the e^-p and e^+p neutral current (NC) DIS cross sections up to Q^2 of 30000 GeV^2 using the data collected in the years 1992–2000, referred to as the HERA I data-taking period. A combination of the results has been published [2].

The combined cross sections were used as the sole input to a next-to-leading order (NLO) quantum chromodynamics (QCD) analysis to determine the set of parton distribution functions (PDFs) called HERAPDF1.0 [2]. The HERA I data were sufficiently precise to demonstrate the effects of Z exchange by comparing the e^-p and e^+p NC DIS cross sections at high Q^2 [2].

HERA underwent a major upgrade before the 2003–2007 data-taking period, referred to as HERA II running. The upgrade significantly increased the instantaneous luminosity delivered by HERA and also provided

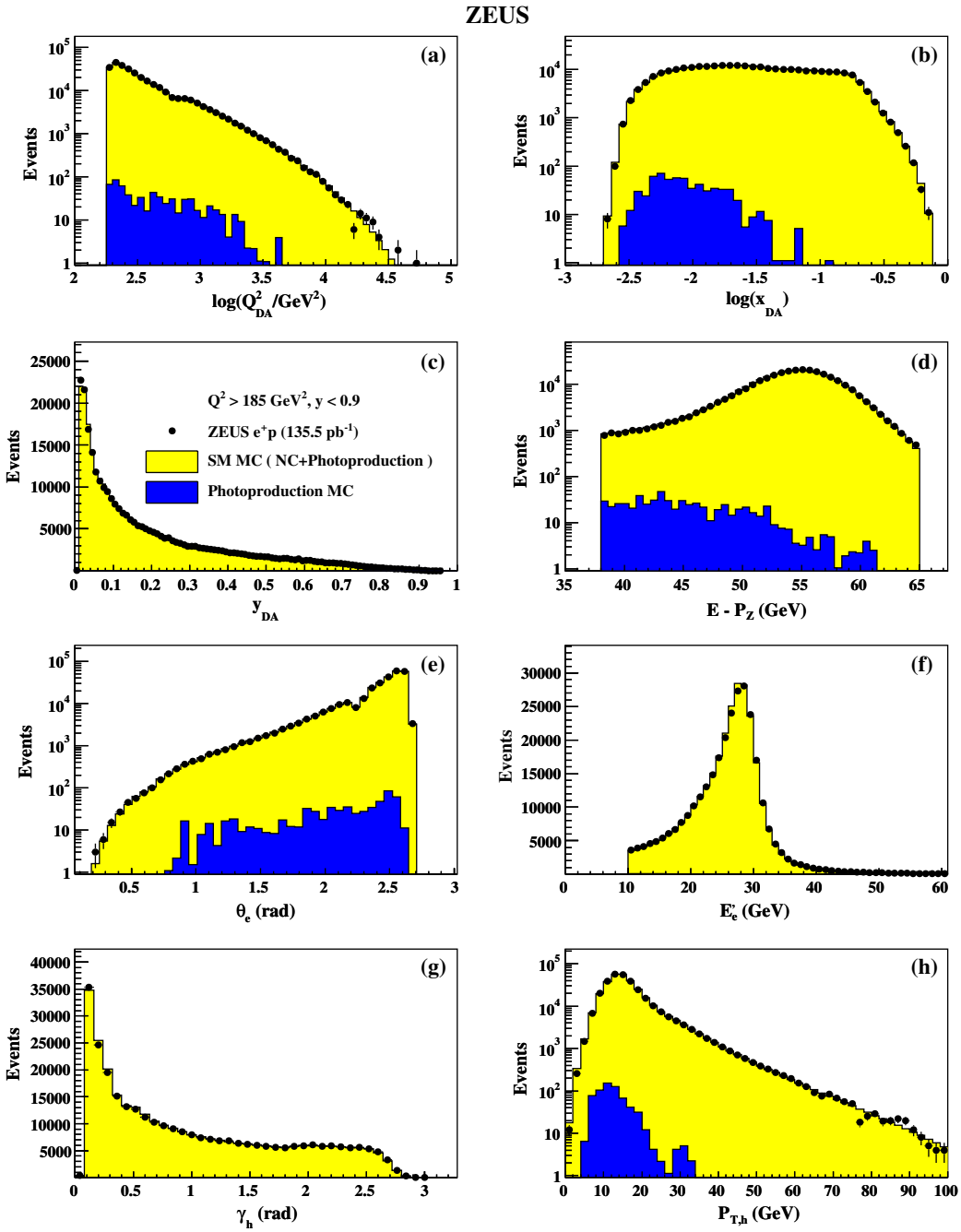

FIG. 1 (color online). Comparison of the e^+p NC data sample with the predictions from the MC simulation. The MC distributions are normalized to the data luminosity. The distributions of (a) Q^2_{DA}, (b) x_{DA}, (c) y_{DA}, (d) $E - P_{\mathrm{Z}}$, (e) θ_{e}, (f) E'_{e}, (g) γ_h and (h) $P_{T,h}$ are shown.

longitudinally polarized electron[1] beams for the collider experiments. The larger collected luminosity provided a higher reach in Q^2 and the longitudinal lepton-beam polarization gave a unique opportunity to study the helicity structure of the electroweak interaction.

The ZEUS Collaboration has already published the NC and charged current (CC) inclusive cross sections for all HERA II running periods except for the NC e^+p data collected in 2006–2007 [3–6]. In this paper, we report NC e^+p cross sections for $Q^2 > 185$ GeV^2 for this period. The H1 Collaboration has recently also published NC and CC cross sections for the HERA II running periods [7].

Parity-violating effects induced by electroweak processes can be demonstrated via the difference between the

[1]In this paper, the word "electron" refers to both electrons and positrons, unless otherwise stated.

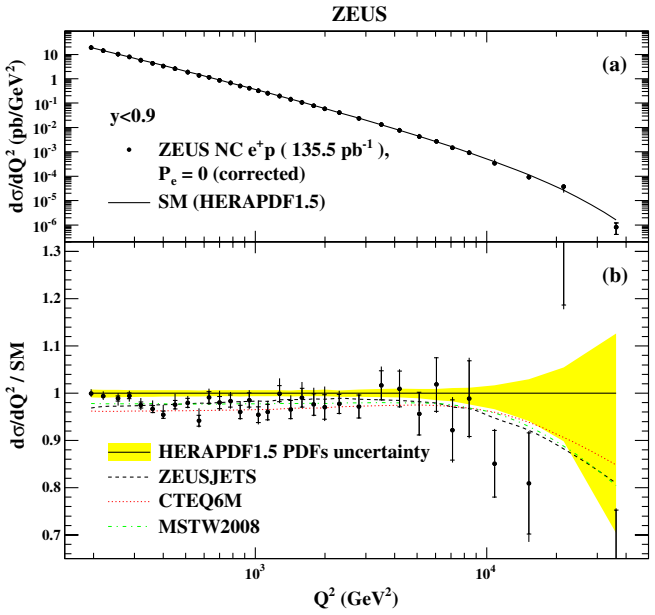

FIG. 2 (color online). (a) The e^+p NC DIS cross-section $d\sigma/dQ^2$ for $y < 0.9$ and $y(1-x)^2 > 0.004$ corrected to $P_e = 0$ and (b) the ratio to SM predictions. The closed circles represent data points in which the inner error bars show the statistical uncertainty while the outer bars show the statistical and systematic uncertainties added in quadrature. The curves show the predictions of the SM evaluated using the HERAPDF1.5 PDFs and the shaded band shows the uncertainties from the HERAPDF1.5 PDFs. In the ratio plot, the ratios between other PDFs [ZEUSJETS (dashed), CTEQ6M (dotted) and MSTW2008 (dash dotted)] and HERAPDF1.5 are shown as curves. The uncertainties of CTEQ6M and MSTW2008 are of the same order as HERAPDF1.5, the uncertainties of ZEUSJETS are about a factor 2 larger.

cross sections involving negatively and positively polarized electron beams. For positrons, this is expressed through the asymmetry parameter A^+, which is proportional to the product of the electron axial (a_e) and quark vector (v_q) couplings to the Z boson. In this paper, the cross sections and the polarization asymmetry are presented and compared to SM predictions, providing a test of the electroweak sector and a key input to further QCD fits.

II. PREDICTIONS FROM THE STANDARD MODEL

Inclusive deep inelastic lepton-proton scattering can be described in terms of the kinematic variables x, y and Q^2. The variable Q^2 is defined as $Q^2 = -q^2 = -(k - k')^2$, where k and k' are the four-momenta of the incoming and scattered lepton, respectively. Bjorken x is defined as $x = Q^2/2P \cdot q$, where P is the four-momentum of the incoming proton. The fraction of the lepton energy transferred to the proton in the rest frame of the proton is given by $y = P \cdot q/P \cdot k$. The variables x, y and Q^2 are related by $Q^2 = sxy$, where s is the square of the lepton-proton center-of-mass energy. At HERA, $s = 4E_eE_p$, where E_e and E_p are the initial electron and proton energies, respectively. The electroweak Born-level cross section for $e^\pm p$ NC interactions can be written as [8,9]

$$\frac{d^2\sigma(e^\pm p)}{dxdQ^2} = \frac{2\pi\alpha^2}{xQ^4}[Y_+\tilde{F}_2(x,Q^2) \mp Y_-x\tilde{F}_3(x,Q^2) - y^2\tilde{F}_L(x,Q^2)], \quad (1)$$

where α is the fine-structure constant, $Y_\pm = 1 \pm (1-y)^2$ and $\tilde{F}_2(x,Q^2)$, $\tilde{F}_3(x,Q^2)$ and $\tilde{F}_L(x,Q^2)$ are generalized structure functions. NLO QCD calculations predict [8,9] and measurements confirm [10,11] that the contribution of the longitudinal structure function $\tilde{F}_L$ to $d^2\sigma/dxdQ^2$ is approximately 1%, averaged over the kinematic range considered here. However, in the high-y region, the $\tilde{F}_L$ contribution to the cross section can be as large as 10% and

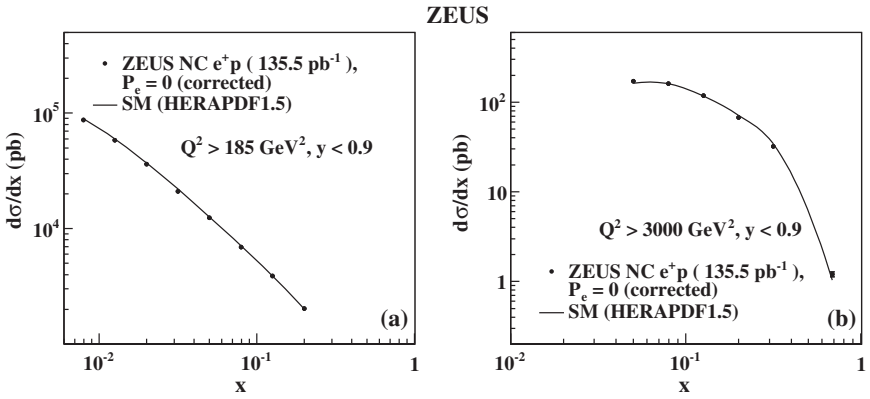

FIG. 3. The e^+p NC DIS cross-section $d\sigma/dx$ for (a) $Q^2 > 185$ GeV^2 and (b) $Q^2 > 3000$ GeV^2 for $y < 0.9$ and $y(1-x)^2 > 0.004$. The closed circles represent data points in which the inner error bars show the statistical uncertainty while the outer bars show the statistical and systematic uncertainties added in quadrature. The curves show the predictions of the SM evaluated using the HERAPDF1.5 PDFs.

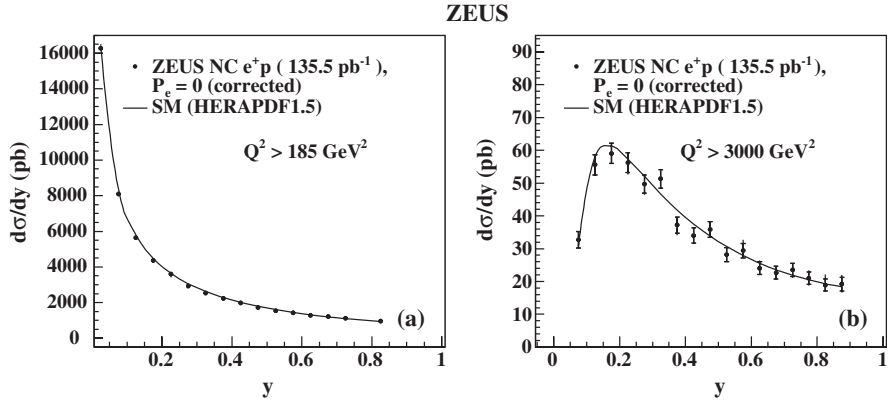

FIG. 4. The e^+p NC DIS cross-section $d\sigma/dy$ for (a) $Q^2 > 185$ GeV^2 and (b) $Q^2 > 3000$ GeV^2 for $y(1-x)^2 > 0.004$. Other details as in Fig. 3.

it is therefore included in the SM predictions compared to the measurements presented in this paper.

The generalized structure functions depend on the longitudinal polarization of the lepton beam, which is defined as

$$P_e = \frac{N_R - N_L}{N_R + N_L}, \tag{2}$$

where N_R and N_L are the numbers of right- and left-handed leptons in the beam.[2]

The $\tilde{F}_2$ term in Eq. (1) is dominant at low Q^2, where only photon exchange is important, while the $\tilde{F}_3$ term starts to contribute significantly to the cross section only at Q^2 values of the order of the mass of the Z boson squared, M_Z^2, and above. It results from γ/Z interference and Z exchange. The sign of the $\tilde{F}_3$ term in Eq. (1) shows that electroweak effects decrease (increase) the e^+p (e^-p) cross section.

The reduced cross sections for e^-p and e^+p scattering are defined as

$$\tilde{\sigma}^{e^\pm p} = \frac{xQ^4}{2\pi\alpha^2}\frac{1}{Y_+}\frac{d^2\sigma(e^\pm p)}{dxdQ^2} = \tilde{F}_2(x,Q^2) \mp \frac{Y_-}{Y_+}x\tilde{F}_3(x,Q^2) - \frac{y^2}{Y_+}F_L(x,Q^2). \tag{3}$$

Thus $x\tilde{F}_3$ can be obtained from the difference of the e^-p and e^+p reduced cross sections as

$$x\tilde{F}_3 = \frac{Y_+}{2Y_-}(\tilde{\sigma}^{e^-p} - \tilde{\sigma}^{e^+p}). \tag{4}$$

The generalized structure functions can be split into terms depending on γ exchange (F_2^γ), Z exchange (F_2^Z, xF_3^Z) and γ/Z interference ($F_2^{\gamma Z}$, $xF_3^{\gamma Z}$) as

$$\tilde{F}_2^\pm = F_2^\gamma - (v_e \pm P_e a_e)\chi_Z F_2^{\gamma Z} + (v_e^2 + a_e^2 \pm 2P_e v_e a_e)\chi_Z^2 F_2^Z, \tag{5}$$

$$x\tilde{F}_3^\pm = -(a_e \pm P_e v_e)\chi_Z x F_3^{\gamma Z} + (2v_e a_e \pm P_e(v_e^2 + a_e^2))\chi_Z^2 x F_3^Z. \tag{6}$$

The SM predictions for the respective vector and axial couplings of the electron to the Z boson are $v_e = -1/2 + 2\sin^2\theta_W$ and $a_e = -1/2$, where θ_W is the Weinberg angle. The relative fraction of events coming from Z with respect to γ exchange is given by

$$\chi_Z = \frac{1}{\sin^2 2\theta_W}\frac{Q^2}{M_Z^2 + Q^2}. \tag{7}$$

This fraction varies between 0.03 and 1.1 over the range of the analysis, 185 GeV$^2 < Q^2 <$ 50000 GeV^2. For the unpolarized case ($P_e = 0$), ignoring terms containing v_e, which is small (≈ -0.04), the interference structure function $xF_3^{\gamma Z}$ is the dominant term in $x\tilde{F}_3$, and

$$x\tilde{F}_3 \simeq -a_e\chi_Z x F_3^{\gamma Z}. \tag{8}$$

The structure functions can be written in terms of the sum and differences of the quark and antiquark momentum distributions. At leading order (LO) in QCD,

$$[F_2^\gamma, F_2^{\gamma Z}, F_2^Z] = \sum_q [e_q^2, 2e_q v_q, v_q^2 + a_q^2]x(q + \bar{q}), \tag{9}$$

$$[xF_3^{\gamma Z}, xF_3^Z] = \sum_q [e_q a_q, v_q a_q] 2x(q - \bar{q}), \tag{10}$$

where v_q and a_q are the respective vector and axial couplings of the quark q to the Z boson, and e_q is the electric charge of the quark. The densities of the quarks and antiquarks are given by q and $\bar{q}$, respectively. The sum runs over all quark flavors except the top quark.

The sensitivity of $xF_3^{\gamma Z}$ to the u and d valence-quark momentum distributions is demonstrated in LO QCD through the expression

[2]At the HERA beam energies, the mass of the incoming leptons can be neglected, and therefore the difference between handedness and helicity can also be neglected.

$$xF_3^{\gamma Z} = 2x[e_u a_u u_v + e_d a_d d_v] = \frac{x}{3}(2u_v + d_v), \quad (11)$$

where the SM values $v_u = 1/2 - 4/3\sin^2\theta_W$ and $a_u = 1/2$ have been used.

The charge-dependent polarization asymmetry, A^+, for a pure right-handed ($P_e = +1$) and left-handed ($P_e = -1$) positron beam is defined as

$$A^+ \equiv \frac{\sigma^+(P_e = +1) - \sigma^+(P_e = -1)}{\sigma^+(P_e = +1) + \sigma^+(P_e = -1)}, \quad (12)$$

where $\sigma^+(P_e = +1)$ and $\sigma^+(P_e = -1)$ are the differential e^+p cross sections evaluated at longitudinal polarization values of $+1$ and -1, respectively. In general, A^+ can be calculated as

$$A^+ = \frac{\sigma^+(P_{e,+}) - \sigma^+(P_{e,-})}{P_{e,+}\sigma^+(P_{e,-}) - P_{e,-}\sigma^+(P_{e,+})}, \quad (13)$$

where $\sigma^+(P_{e,+})$ and $\sigma^+(P_{e,-})$ are the differential e^+p cross sections evaluated at any positive and negative polarization values. For $P_{e,+} \approx -P_{e,-}$ this equation becomes

$$A^+ = \frac{2}{P_{e,+} - P_{e,-}} \cdot \frac{\sigma^+(P_{e,+}) - \sigma^+(P_{e,-})}{\sigma^+(P_{e,+}) + \sigma^+(P_{e,-})}. \quad (14)$$

Keeping only the leading terms, A^+ can be written as

$$A^+ \simeq -\chi_Z a_e \frac{F_2^{\gamma Z}}{F_2^{\gamma}} = -2\chi_Z a_e v_q e_q / e_q^2 \propto a_e v_q. \quad (15)$$

As the asymmetry parameter is proportional to the ratio of the $F_2^{\gamma Z}$ and F_2^{γ} structure functions, it is to first order insensitive to PDFs. Therefore a measurement of A^+ can give direct evidence of parity violation with minimal assumptions on the proton structure. As, in the SM, A^+ is expected to be a small quantity, less than 10% for Q^2 values below 2000 GeV^2, increasing slowly to 30% by Q^2 of 10000 GeV^2, precise measurements of the polarized cross sections are required.

III. EXPERIMENTAL SETUP

The analysis is based on a data sample collected from 2006–2007, when HERA collided positrons of energy $E_e = 27.5$ GeV with protons of energy $E_p = 920$ GeV, corresponding to a center-of-mass energy $\sqrt{s} = 318$ GeV. The total integrated luminosity of the sample is 135.5 ± 2.5 pb^{-1}, of which 78.8 ± 1.4 pb^{-1} were collected at a luminosity-weighted lepton-beam polarization $P_e = 0.32 \pm 0.01$ and 56.7 ± 1.1 pb^{-1} at $P_e = -0.36 \pm 0.01$.

A detailed description of the ZEUS detector can be found elsewhere [12]. A brief outline of the components that are most relevant for this analysis is given below.

Charged particles were tracked in the central tracking detector (CTD) [13]which operated in a magnetic field of 1.43 T provided by a thin superconducting solenoid. The CTD consisted of 72 cylindrical drift chamber layers organized in nine superlayers covering the polar-angle[3] region $15° < \theta < 164°$. The CTD was complemented by a silicon microvertex detector (MVD) [14] consisting of three active layers in the barrel and four disks in the forward region. For CTD-MVD tracks that pass through all nine CTD superlayers, the momentum resolution was $\sigma(p_T)/p_T = 0.0029p_T \oplus 0.0081 \oplus 0.0012/p_T$, with p_T in GeV.

The high-resolution uranium-scintillator calorimeter (CAL) [15] consisted of three parts: the forward (FCAL), the barrel (BCAL) and the rear (RCAL) calorimeters. Each part was subdivided transversely into towers and longitudinally into one electromagnetic section and either one (in RCAL) or two (in BCAL and FCAL) hadronic sections. The smallest subdivision of the calorimeter is called a cell. The CAL energy resolutions, as measured under test-beam conditions, were $\sigma(E)/E = 0.18/\sqrt{E}$ for electrons and $\sigma(E)/E = 0.35/\sqrt{E}$ for hadrons, with E in GeV.

The luminosity was measured using the Bethe-Heitler reaction $ep \to e\gamma p$ by a luminosity detector which consisted of independent lead-scintillator calorimeter [16] and magnetic spectrometer [17] systems. The fractional systematic uncertainty on the measured luminosity was 1.8% for the period with $P_e = 0.32$ and 1.9% for the period with $P_e = -0.36$.

The lepton beam in HERA became naturally transversely polarized through the Sokolov-Ternov effect [18]. The characteristic buildup time in HERA was approximately 40 minutes. Spin rotators on either side of the ZEUS detector changed the transverse polarization of the beam into longitudinal polarization and back to transverse. The electron beam polarization was measured using two independent polarimeters, the transverse polarimeter [19,20] and the longitudinal polarimeter [21]. Both devices exploited the spin-dependent cross section for Compton scattering of circularly polarized photons off electrons to measure the beam polarization. The luminosity and polarization measurements were made over time scales that were much shorter than the polarization buildup time.

IV. MONTE CARLO SIMULATION

Monte Carlo (MC) simulations were used to determine the efficiency of the event selection, the accuracy of the kinematic reconstruction, to estimate the background rate and to extrapolate the measured cross sections to the full kinematic region. The effective luminosities of the MC samples were at least five times larger than that of the

[3]The ZEUS coordinate system is a right-handed Cartesian system, with the Z axis pointing in the proton beam direction referred to as the "forward direction," and the X axis pointing towards the center of HERA. The coordinate origin is at the nominal interaction point. The pseudorapidity is defined as $\eta = -\ln(\tan(\theta/2))$, where the polar angle θ is measured with respect to the proton beam direction.

TABLE I. The single-differential cross-section $d\sigma/dQ^2$ [$y < 0.9$, $y(1-x)^2 > 0.004$] for the reaction $e^+p \to e^+X$ ($\mathcal{L} = 135.5$ pb^{-1} corrected to $P_e = 0$). The bin range, bin center (Q_c^2) and measured cross section corrected to the electroweak Born level are shown. The first (second) error on the cross section corresponds to the statistical (systematic) uncertainties. The number of observed data events (N_{data}) and simulated background events ($N_{\text{bg}}^{\text{MC}}$) are also shown.

Q^2 range (GeV^2)	Q_c^2 (GeV^2)	$d\sigma/dQ^2$ (pb/GeV^2)	N_{data}	$N_{\text{bg}}^{\text{MC}}$
185–210	195	$(1.91 \pm 0.01^{+0.01}_{-0.01}) \times 10^1$	55281	110.7
210–240	220	$(1.43 \pm 0.01^{+0.01}_{-0.01}) \times 10^1$	47861	71.9
240–270	255	$(1.01 \pm 0.01^{+0.01}_{-0.01}) \times 10^1$	34808	58.9
270–300	285	$(7.79 \pm 0.05^{+0.07}_{-0.09})$	25835	22.3
300–340	320	$(5.79 \pm 0.04^{+0.08}_{-0.05})$	24184	36.0
340–380	360	$(4.35 \pm 0.03^{+0.07}_{-0.02})$	17201	21.9
380–430	400	$(3.33 \pm 0.03^{+0.07}_{-0.02})$	15791	29.3
430–480	450	$(2.56 \pm 0.02^{+0.06}_{-0.01})$	11903	38.5
480–540	510	$(1.89 \pm 0.02^{+0.02}_{-0.01})$	10365	20.7
540–600	570	$(1.39 \pm 0.02^{+0.03}_{-0.01})$	6943	38.7
600–670	630	$(1.14 \pm 0.01^{+0.02}_{-0.01})$	6366	19.7
670–740	700	$(8.70 \pm 0.12^{+0.19}_{-0.10}) \times 10^{-1}$	5655	23.0
740–820	780	$(6.65 \pm 0.09^{+0.10}_{-0.06}) \times 10^{-1}$	5750	19.6
820–900	860	$(5.08 \pm 0.07^{+0.10}_{-0.05}) \times 10^{-1}$	4654	24.5
900–990	940	$(4.16 \pm 0.06^{+0.06}_{-0.05}) \times 10^{-1}$	4295	15.6
990–1080	1030	$(3.20 \pm 0.06^{+0.09}_{-0.04}) \times 10^{-1}$	3304	10.3
1080–1200	1130	$(2.55 \pm 0.04^{+0.05}_{-0.03}) \times 10^{-1}$	3522	18.1
1200–1350	1270	$(1.96 \pm 0.03^{+0.06}_{-0.02}) \times 10^{-1}$	3439	14.0
1350–1500	1420	$(1.42 \pm 0.03^{+0.03}_{-0.01}) \times 10^{-1}$	2501	16.9
1500–1700	1590	$(1.08 \pm 0.02^{+0.03}_{-0.01}) \times 10^{-1}$	2549	9.3
1700–1900	1790	$(7.84 \pm 0.18^{+0.22}_{-0.08}) \times 10^{-2}$	1849	8.5
1900–2100	1990	$(5.88 \pm 0.16^{+0.21}_{-0.09}) \times 10^{-2}$	1393	8.3
2100–2600	2300	$(4.02 \pm 0.08^{+0.08}_{-0.04}) \times 10^{-2}$	2311	7.2
2600–3200	2800	$(2.34 \pm 0.06^{+0.03}_{-0.02}) \times 10^{-2}$	1565	3.0
3200–3900	3500	$(1.31 \pm 0.04^{+0.03}_{-0.01}) \times 10^{-2}$	1083	1.3
3900–4700	4200	$(7.77 \pm 0.29^{+0.14}_{-0.10}) \times 10^{-3}$	715	3.9
4700–5600	5100	$(4.18 \pm 0.20^{+0.04}_{-0.06}) \times 10^{-3}$	447	0.0
5600–6600	6050	$(2.66 \pm 0.15^{+0.03}_{-0.05}) \times 10^{-3}$	320	0.0
6600–7800	7100	$(1.47 \pm 0.10^{+0.05}_{-0.04}) \times 10^{-3}$	208	0.0
7800–9200	8400	$(9.20 \pm 0.75^{+0.31}_{-0.22}) \times 10^{-4}$	152	0.0
9200–12800	10800	$(3.40 \pm 0.28^{+0.09}_{-0.06}) \times 10^{-4}$	145	0.0
12800–18100	15200	$(9.21 \pm 1.22^{+0.31}_{-0.71}) \times 10^{-5}$	57	0.0
18100–25600	21500	$(3.81^{+0.76+0.23}_{-0.64-0.17}) \times 10^{-5}$	35	0.0
25600–50000	36200	$(8.23^{+6.51+0.71}_{-3.94-0.59}) \times 10^{-7}$	4	0.0

TABLE II. The single-differential cross-section $d\sigma/dx$ [$y < 0.9$, $y(1-x)^2 > 0.004$] for $Q^2 > 185$ GeV^2 and $Q^2 > 3000$ GeV^2 for the reaction $e^+p \to e^+X$ ($\mathcal{L} = 135.5$ pb^{-1} corrected to $P_e = 0$). The Q^2 and bin range, bin center (x_c) and measured cross section corrected to the electroweak Born level are shown. Other details as in Table I.

$Q^2>$ (GeV^2)	x range	x_c	$d\sigma/dx$ (pb)	N_{data}	$N_{\text{bg}}^{\text{MC}}$
185	$(0.63-1.00)\times10^{-2}$	0.794×10^{-2}	$(8.71\pm0.05^{+0.14}_{-0.10})\times10^4$	34570	164.3
	$(0.10-0.16)\times10^{-1}$	0.126×10^{-1}	$(5.84\pm0.03^{+0.07}_{-0.07})\times10^4$	39862	124.8
	$(0.16-0.25)\times10^{-1}$	0.200×10^{-1}	$(3.62\pm0.02^{+0.03}_{-0.02})\times10^4$	39233	85.4
	$(0.25-0.40)\times10^{-1}$	0.316×10^{-1}	$(2.10\pm0.01^{+0.04}_{-0.01})\times10^4$	38384	29.6
	$(0.40-0.63)\times10^{-1}$	0.501×10^{-1}	$(1.24\pm0.01^{+0.02}_{-0.01})\times10^4$	33557	5.5
	$(0.63-1.00)\times10^{-1}$	0.794×10^{-1}	$(6.90\pm0.04^{+0.11}_{-0.03})\times10^3$	31825	5.1
	0.10–0.16	0.126	$(3.89\pm0.02^{+0.06}_{-0.02})\times10^3$	30244	2.0
	0.16–0.25	0.200	$(2.04\pm0.01^{+0.04}_{-0.03})\times10^3$	18768	0.0
3000	$(0.40-0.63)\times10^{-1}$	0.501×10^{-1}	$(1.71\pm0.08^{+0.06}_{-0.03})\times10^2$	440	1.3
	$(0.63-1.00)\times10^{-1}$	0.794×10^{-1}	$(1.60\pm0.06^{+0.04}_{-0.02})\times10^2$	714	3.9
	0.10–0.16	0.126	$(1.18\pm0.04^{+0.01}_{-0.02})\times10^2$	859	0.0
	0.16—0.25	0.200	$(6.72\pm0.25^{+0.06}_{-0.08})\times10^1$	730	0.0
	0.25–0.40	0.316	$(3.22\pm0.14^{+0.04}_{-0.03})\times10^1$	567	0.0
	0.40–0.75	0.687	$(1.20\pm0.08^{+0.02}_{-0.03})$	240	0.0

data sample and were normalized to the total integrated luminosity of the data.

Neutral current DIS events were simulated, including radiative effects, using the HERACLES [22] program with the DJANGOH 1.6 [23] interface to the hadronization programs and using the CTEQ5D [24] PDFs. The hadronic final state was simulated using the color-dipole model of ARIADNE 4.12 [25]. To investigate systematic uncertainties, the MEPS model of LEPTO 6.5 [26] was also used. The Lund string model of JETSET 7.4 [27] was used for the hadronization. Photoproduction (γp) events were simulated using HERWIG 5.9 [28] to study this background.

The ZEUS detector response was simulated using a program based on GEANT 3.21 [29]. The generated events were passed through the detector simulation, subjected to the same trigger requirements as the data and processed by the same reconstruction programs.

The distribution of the Z position of the interactions was a crucial input to the MC simulation with which the event-selection efficiency was determined. In order to measure this distribution, a special NC DIS sample was selected, for which the event-selection efficiency did not depend on the Z of the interaction [30].

V. EVENT RECONSTRUCTION

Neutral current events at high Q^2 are characterized by the presence of an isolated high-energy electron in the final state. The transverse momentum of the scattered electron balances that of the hadronic final state. Therefore the net transverse momentum of the event P_T representing the vectorial sum of the transverse momenta of all particles, $\vec{p}_T$ should be small. The measured net P_T and transverse energy, E_T were calculated as

$$P_T^2 = P_X^2 + P_Y^2 = \left(\sum_i E_i \sin\theta_i \cos\phi_i\right)^2 + \left(\sum_i E_i \sin\theta_i \sin\phi_i\right)^2,$$
$$E_T = \sum_i E_i \sin\theta_i, \tag{16}$$

where the sum ran over all calorimeter energy deposits E_i, and the polar (θ_i) and azimuthal (ϕ_i) angles were measured with respect to the interaction vertex. The variable δ defined as

$$\delta \equiv \sum_i (E - P_Z)_i = \sum_i (E_i - E_i\cos\theta_i) \equiv E - P_Z \tag{17}$$

was also used in the event selection. Conservation of energy and longitudinal momentum implies that $\delta = 2E_e = 55$ GeV, if all final-state particles were detected and perfectly measured. Undetected particles that escape through the forward beam hole had a negligible effect on δ. However, particles lost through the rear beam hole could lead to a substantial reduction in δ. This was the case for γp events, where the electron emerged at a very small scattering angle, or for events in which an initial-state bremsstrahlung photon was emitted.

The CAL energy deposits were separated into those associated with the scattered electron and all other energy deposits. The sum of the latter was called the hadronic energy. The hadronic polar angle γ_h was defined as

TABLE III. The single-differential cross-section $d\sigma/dy$ for $Q^2 > 185$ GeV^2 and $Q^2 > 3000$ GeV^2 $[y(1-x)^2 > 0.004]$ for the reaction $e^+p \to e^-X$ ($\mathcal{L} = 135.5$ pb^{-1} corrected to $P_e = 0$). The Q^2 and bin range, bin center (y_c) and measured cross section corrected to the electroweak Born level are shown. Other details as in Table I.

$Q^2>$ (GeV^2)	y range	y_c	$d\sigma/dy$ (pb)	N_{data}	$N_{\text{bg}}^{\text{MC}}$
185	0.00–0.05	0.025	$(1.63 \pm 0.01^{+0.02}_{-0.01}) \times 10^4$	75314	0.0
	0.05–0.10	0.075	$(8.10 \pm 0.04^{+0.14}_{-0.05}) \times 10^3$	50532	7.4
	0.10–0.15	0.125	$(5.64 \pm 0.03^{+0.03}_{-0.04}) \times 10^3$	34944	15.0
	0.15–0.20	0.175	$(4.37 \pm 0.03^{+0.02}_{-0.05}) \times 10^3$	26237	23.7
	0.20–0.25	0.225	$(3.61 \pm 0.03^{+0.03}_{-0.04}) \times 10^3$	20974	19.1
	0.25–0.30	0.275	$(2.93 \pm 0.02^{+0.04}_{-0.03}) \times 10^3$	16254	18.5
	0.30–0.35	0.325	$(2.53 \pm 0.02^{+0.04}_{-0.02}) \times 10^3$	13919	43.8
	0.35–0.40	0.375	$(2.24 \pm 0.02^{+0.02}_{-0.03}) \times 10^3$	12202	48.2
	0.40–0.45	0.425	$(1.98 \pm 0.02^{+0.03}_{-0.02}) \times 10^3$	10402	63.7
	0.45–0.50	0.475	$(1.73 \pm 0.02^{+0.05}_{-0.02}) \times 10^3$	8761	48.5
	0.50–0.55	0.525	$(1.54 \pm 0.02^{+0.04}_{-0.01}) \times 10^3$	7661	55.7
	0.55–0.60	0.575	$(1.42 \pm 0.02^{+0.04}_{-0.02}) \times 10^3$	6794	61.4
	0.60–0.65	0.625	$(1.29 \pm 0.02^{+0.04}_{-0.02}) \times 10^3$	5723	61.4
	0.65–0.70	0.675	$(1.21 \pm 0.02^{+0.04}_{-0.03}) \times 10^3$	4671	24.9
	0.70–0.75	0.725	$(1.12 \pm 0.02^{+0.07}_{-0.03}) \times 10^3$	3542	47.8
	0.75–0.90	0.825	$(9.53 \pm 0.14^{+0.77}_{-0.30}) \times 10^2$	4433	109.1
3000	0.05–0.10	0.075	$(3.27 \pm 0.25^{+0.06}_{-0.06}) \times 10^1$	174	0.0
	0.10–0.15	0.125	$(5.56 \pm 0.31^{+0.05}_{-0.04}) \times 10^1$	326	0.0
	0.15–0.20	0.175	$(5.91 \pm 0.31^{+0.07}_{-0.09}) \times 10^1$	357	0.0
	0.20–0.25	0.225	$(5.62 \pm 0.30^{+0.05}_{-0.08}) \times 10^1$	345	0.0
	0.25–0.30	0.275	$(4.97 \pm 0.28^{+0.04}_{-0.08}) \times 10^1$	312	0.0
	0.30–0.35	0.325	$(5.13 \pm 0.29^{+0.05}_{-0.07}) \times 10^1$	321	0.0
	0.35–0.40	0.375	$(3.72 \pm 0.24^{+0.04}_{-0.08}) \times 10^1$	233	0.0
	0.40–0.45	0.425	$(3.40 \pm 0.23^{+0.04}_{-0.09}) \times 10^1$	214	0.0
	0.45–0.50	0.475	$(3.59 \pm 0.24^{+0.04}_{-0.08}) \times 10^1$	224	0.0
	0.50–0.55	0.525	$(2.82 \pm 0.21^{+0.03}_{-0.08}) \times 10^1$	173	0.0
	0.55–0.60	0.575	$(2.94 \pm 0.22^{+0.26}_{-0.04}) \times 10^1$	178	0.0
	0.60–0.65	0.625	$(2.41 \pm 0.20^{+0.15}_{-0.04}) \times 10^1$	152	3.9
	0.65–0.70	0.675	$(2.27 \pm 0.20^{+0.06}_{-0.07}) \times 10^1$	134	0.0
	0.70–0.75	0.725	$(2.35 \pm 0.20^{+0.05}_{-0.10}) \times 10^1$	134	0.0
	0.75–0.80	0.775	$(2.10 \pm 0.19^{+0.14}_{-0.07}) \times 10^1$	119	0.2
	0.80–0.85	0.825	$(1.89 \pm 0.19^{+0.26}_{-0.04}) \times 10^1$	103	1.1
	0.85–0.90	0.875	$(1.92 \pm 0.21^{+0.13}_{-0.16}) \times 10^1$	87	0.0

$$\cos\gamma_h = \frac{P_{T,h}^2 - \delta_h^2}{P_{T,h}^2 + \delta_h^2}, \tag{18}$$

where the quantities $P_{T,h}$ and δ_h were derived from Eqs. (16) and (17) using only the hadronic energy. In the naive quark-parton model, γ_h is the angle by which the struck quark is scattered.

The double angle (DA) method [31] used the polar angle of the scattered electron, θ_e, and the hadronic angle, γ_h, to reconstruct the kinematic variables x_{DA}, y_{DA} and Q^2_{DA}. For the determination of θ_e, tracking information was also used

TABLE IV. The reduced cross-section $\tilde{\sigma}$ for the reaction $e^+ p \to e^+ X$ ($\mathcal{L} = 135.5$ pb^{-1} corrected to $P_e = 0$). The bin range, bin center (Q_c^2 and x_c) and measured cross section corrected to the electroweak Born level are shown. Other details as in Table I. This table has one continuation.

Q^2 range (GeV^2)	Q_c^2 (GeV^2)	x range	x_c	$\tilde{\sigma}$	N_{data}	$N_{\text{bg}}^{\text{MC}}$
185–240	200	0.004 − 0.006	0.005	$(1.110 \pm 0.010^{+0.025}_{-0.020})$	13313	110.0
	200	0.006 − 0.010	0.008	$(0.945 \pm 0.008^{+0.008}_{-0.018})$	15647	36.5
	200	0.010 − 0.017	0.013	$(0.801 \pm 0.006^{+0.002}_{-0.014})$	16074	13.7
	200	0.017 − 0.025	0.021	$(0.680 \pm 0.006^{+0.005}_{-0.004})$	11107	5.1
	200	0.025 − 0.037	0.032	$(0.566 \pm 0.006^{+0.014}_{-0.001})$	9767	0.0
	200	0.037 − 0.060	0.050	$(0.511 \pm 0.005^{+0.012}_{-0.002})$	10375	1.1
	200	0.060 − 0.120	0.080	$(0.433 \pm 0.004^{+0.012}_{-0.001})$	13867	0.0
	200	0.120 − 0.250	0.180	$(0.346 \pm 0.004^{+0.006}_{-0.004})$	8823	0.0
240–310	250	0.006 − 0.010	0.008	$(0.929 \pm 0.010^{+0.022}_{-0.007})$	9190	35.7
	250	0.010 − 0.017	0.013	$(0.821 \pm 0.008^{+0.006}_{-0.012})$	10611	10.3
	250	0.017 − 0.025	0.021	$(0.692 \pm 0.008^{+0.005}_{-0.009})$	7770	8.5
	250	0.025 − 0.037	0.032	$(0.585 \pm 0.007^{+0.010}_{-0.011})$	7466	1.1
	250	0.037 − 0.060	0.050	$(0.513 \pm 0.006^{+0.014}_{-0.008})$	7740	0.0
	250	0.060 − 0.120	0.080	$(0.435 \pm 0.004^{+0.009}_{-0.005})$	10142	0.0
	250	0.120 − 0.250	0.180	$(0.337 \pm 0.004^{+0.005}_{-0.008})$	8042	0.0
310–410	350	0.006 − 0.010	0.008	$(0.948 \pm 0.013^{+0.025}_{-0.008})$	5579	26.7
	350	0.010 − 0.017	0.013	$(0.809 \pm 0.010^{+0.009}_{-0.003})$	7000	7.9
	350	0.017 − 0.025	0.021	$(0.673 \pm 0.009^{+0.010}_{-0.003})$	5167	0.4
	350	0.025 − 0.037	0.032	$(0.575 \pm 0.008^{+0.015}_{-0.004})$	4869	1.1
	350	0.037 − 0.060	0.050	$(0.507 \pm 0.007^{+0.010}_{-0.005})$	5306	1.1
	350	0.060 − 0.120	0.080	$(0.418 \pm 0.005^{+0.014}_{-0.004})$	6823	0.0
	350	0.120 − 0.250	0.180	$(0.325 \pm 0.004^{+0.005}_{-0.005})$	6340	0.0
410–530	450	0.006 − 0.010	0.008	$(1.023 \pm 0.015^{+0.020}_{-0.017})$	4548	45.7
	450	0.010 − 0.017	0.013	$(0.816 \pm 0.014^{+0.010}_{-0.009})$	3304	7.2
	450	0.017 − 0.025	0.021	$(0.706 \pm 0.014^{+0.012}_{-0.004})$	2711	2.2
	450	0.025 − 0.037	0.032	$(0.582 \pm 0.011^{+0.011}_{-0.004})$	2962	1.1
	450	0.037 − 0.060	0.050	$(0.511 \pm 0.008^{+0.010}_{-0.003})$	3618	0.0
	450	0.060 − 0.100	0.080	$(0.425 \pm 0.007^{+0.007}_{-0.002})$	3305	0.0
	450	0.100 − 0.170	0.130	$(0.365 \pm 0.007^{+0.009}_{-0.000})$	3094	0.0
	450	0.170 − 0.300	0.250	$(0.257 \pm 0.005^{+0.007}_{-0.001})$	2612	0.0
530–710	650	0.010 − 0.017	0.013	$(0.865 \pm 0.014^{+0.024}_{-0.015})$	4045	28.7
	650	0.017 − 0.025	0.021	$(0.735 \pm 0.015^{+0.008}_{-0.008})$	2564	0.0
	650	0.025 − 0.037	0.032	$(0.609 \pm 0.013^{+0.015}_{-0.005})$	2043	1.1
	650	0.037 − 0.060	0.050	$(0.512 \pm 0.011^{+0.003}_{-0.004})$	2028	0.0
	650	0.060 − 0.100	0.080	$(0.434 \pm 0.010^{+0.002}_{-0.003})$	1809	0.0
	650	0.100 − 0.170	0.130	$(0.335 \pm 0.008^{+0.009}_{-0.001})$	1598	0.0
	650	0.170 − 0.300	0.250	$(0.238 \pm 0.006^{+0.003}_{-0.003})$	1453	0.0
710–900	800	0.009 − 0.017	0.013	$(0.836 \pm 0.017^{+0.027}_{-0.013})$	2600	41.7
	800	0.017 − 0.025	0.021	$(0.741 \pm 0.018^{+0.009}_{-0.010})$	1757	3.3
	800	0.025 − 0.037	0.032	$(0.610 \pm 0.015^{+0.007}_{-0.006})$	1747	7.9
	800	0.037 − 0.060	0.050	$(0.514 \pm 0.012^{+0.010}_{-0.005})$	1966	0.8
	800	0.060 − 0.100	0.080	$(0.454 \pm 0.011^{+0.003}_{-0.004})$	1768	0.0
	800	0.100 − 0.170	0.130	$(0.344 \pm 0.009^{+0.007}_{-0.002})$	1387	0.0
	800	0.170 − 0.300	0.250	$(0.243 \pm 0.007^{+0.008}_{-0.002})$	1110	0.0
900–1300	1200	0.010 − 0.017	0.014	$(0.816 \pm 0.021^{+0.073}_{-0.025})$	1631	35.8
	1200	0.017 − 0.025	0.021	$(0.738 \pm 0.017^{+0.018}_{-0.011})$	1819	12.0
	1200	0.025 − 0.037	0.032	$(0.626 \pm 0.014^{+0.007}_{-0.008})$	1863	0.0

TABLE IV. (*Continued*)

Q^2 range (GeV^2)	Q_c^2 (GeV^2)	x range	x_c	$\tilde{\sigma}$	N_{data}	$N_{\text{bg}}^{\text{MC}}$
	1200	0.037 − 0.060	0.050	$(0.513 \pm 0.011^{+0.008}_{-0.005})$	2209	0.0
	1200	0.060 − 0.100	0.080	$(0.423 \pm 0.009^{+0.005}_{-0.003})$	2037	1.1
	1200	0.100 − 0.170	0.130	$(0.352 \pm 0.008^{+0.003}_{-0.003})$	1845	0.0
	1200	0.170 − 0.300	0.250	$(0.247 \pm 0.006^{+0.002}_{-0.002})$	1459	0.0
	1200	0.300 − 0.530	0.400	$(0.129 \pm 0.005^{+0.001}_{-0.001})$	624	0.0
1300–1800	1500	0.017 − 0.025	0.021	$(0.724 \pm 0.024^{+0.086}_{-0.014})$	924	17.5
	1500	0.025 − 0.037	0.032	$(0.583 \pm 0.019^{+0.026}_{-0.007})$	952	1.9
	1500	0.037 − 0.060	0.050	$(0.532 \pm 0.015^{+0.005}_{-0.009})$	1309	1.1
	1500	0.060 − 0.100	0.080	$(0.446 \pm 0.012^{+0.005}_{-0.004})$	1303	0.0
	1500	0.100 − 0.150	0.130	$(0.372 \pm 0.012^{+0.004}_{-0.003})$	902	0.9
	1500	0.150 − 0.230	0.180	$(0.306 \pm 0.011^{+0.003}_{-0.002})$	789	0.0
	1500	0.230 − 0.350	0.250	$(0.242 \pm 0.011^{+0.005}_{-0.002})$	528	0.0
	1500	0.350 − 0.530	0.400	$(0.119 \pm 0.007^{+0.002}_{-0.003})$	251	0.0
1800–2500	2000	0.023 − 0.037	0.032	$(0.594 \pm 0.023^{+0.065}_{-0.012})$	701	12.2
	2000	0.037 − 0.060	0.050	$(0.496 \pm 0.018^{+0.010}_{-0.006})$	790	1.1
	2000	0.060 − 0.100	0.080	$(0.474 \pm 0.015^{+0.004}_{-0.005})$	940	1.1
	2000	0.100 − 0.150	0.130	$(0.352 \pm 0.014^{+0.005}_{-0.003})$	607	1.1
	2000	0.150 − 0.230	0.180	$(0.273 \pm 0.012^{+0.003}_{-0.005})$	499	0.0
	2000	0.230 − 0.350	0.250	$(0.247 \pm 0.013^{+0.004}_{-0.006})$	387	0.0
	2000	0.350 − 0.530	0.400	$(0.119 \pm 0.009^{+0.003}_{-0.001})$	180	0.0
2500–3500	3000	0.037 − 0.060	0.050	$(0.500 \pm 0.022^{+0.012}_{-0.010})$	502	2.1
	3000	0.060 − 0.100	0.080	$(0.429 \pm 0.018^{+0.004}_{-0.005})$	575	0.0
	3000	0.100 − 0.150	0.130	$(0.366 \pm 0.017^{+0.007}_{-0.005})$	448	0.0
	3000	0.150 − 0.230	0.180	$(0.276 \pm 0.015^{+0.007}_{-0.005})$	356	0.0
	3000	0.230 − 0.350	0.250	$(0.243 \pm 0.014^{+0.002}_{-0.005})$	286	0.0
	3000	0.350 − 0.530	0.400	$(0.121 \pm 0.011^{+0.004}_{-0.004})$	127	0.0
	3000	0.530 − 0.750	0.650	$(0.015^{+0.004\ +0.001}_{-0.003\ -0.000})$	21	0.0
3500–5600	5000	0.040 − 0.100	0.080	$(0.405 \pm 0.016^{+0.017}_{-0.007})$	628	3.9
	5000	0.100 − 0.150	0.130	$(0.328 \pm 0.018^{+0.003}_{-0.004})$	344	0.0
	5000	0.150 − 0.230	0.180	$(0.286 \pm 0.016^{+0.002}_{-0.007})$	333	0.0
	5000	0.230 − 0.350	0.250	$(0.215 \pm 0.014^{+0.002}_{-0.002})$	232	0.0
	5000	0.350 − 0.530	0.400	$(0.135 \pm 0.012^{+0.002}_{-0.002})$	137	0.0
5600–9000	8000	0.070 − 0.150	0.130	$(0.312 \pm 0.019^{+0.011}_{-0.010})$	277	0.0
	8000	0.150 − 0.230	0.180	$(0.239 \pm 0.019^{+0.002}_{-0.007})$	161	0.0
	8000	0.230 − 0.350	0.250	$(0.213 \pm 0.018^{+0.004}_{-0.005})$	136	0.0
	8000	0.350 − 0.530	0.400	$(0.104 \pm 0.013^{+0.003}_{-0.003})$	66	0.0
	8000	0.530 − 0.750	0.650	$(0.017^{+0.006\ +0.002}_{-0.004\ -0.001})$	15	0.0
9000–1500	12000	0.090 − 0.230	0.180	$(0.192 \pm 0.020^{+0.004}_{-0.004})$	95	0.0
	12000	0.230 − 0.350	0.250	$(0.152 \pm 0.020^{+0.002}_{-0.007})$	56	0.0
	12000	0.350 − 0.530	0.400	$(0.115 \pm 0.017^{+0.004}_{-0.004})$	44	0.0
15000–25000	20000	0.150 − 0.350	0.250	$(0.154^{+0.029\ +0.012}_{-0.025\ -0.005})$	38	0.0
	20000	0.350 − 0.750	0.400	$(0.064^{+0.021\ +0.005}_{-0.016\ -0.012})$	15	0.0
25000–50000	30000	0.250 − 0.750	0.400	$(0.040^{+0.024\ +0.001}_{-0.016\ -0.005})$	6	0.0

when available. The DA method was insensitive to uncertainties in the overall energy scale of the calorimeter. However, it was sensitive to initial-state quantum electrodynamics (QED) radiation and an accurate simulation of the detector response was necessary. The variable y was reconstructed using the electron method (y_e). The Jacquet-Blondel method (y_{JB}) [32] was used in the event selection in kinematic regions where it provided better resolution.

VI. EVENT SELECTION

A. Trigger requirements

Events were selected using a three-level trigger system [12,33,34]. At the first level, only coarse calorimeter and tracking information was available. Events were selected if they had an energy deposit in the CAL consistent with an isolated electron. In addition, events with high E_T or high energy in the electromagnetic part of the calorimeter in coincidence with a CTD track were selected. At the second level, a requirement on δ was used to select NC DIS events. Timing information from the calorimeter was used to reject events inconsistent with the bunch-crossing time. At the third level, events were fully reconstructed. The requirements were similar to, but looser than the off-line cuts described below.

B. Off-line requirements

The following criteria were imposed to select NC events.

(i) Electron identification:
An algorithm which combined information from the energy deposits in the calorimeter with tracks measured in the central tracking detectors was used to identify the scattered electron [35]. To ensure a high purity and to reject background, the identified electron was required to have an energy, E'_e of at least 10 GeV and to be isolated such that the energy not associated with the electron in an η-ϕ cone of radius 0.8 centered on the electron was less than 5 GeV.
A track matched to the energy deposit in the calorimeter was required for events in which an electron was found within the region of good acceptance of the tracking detectors, which was $0.3 < \theta < 2.5$

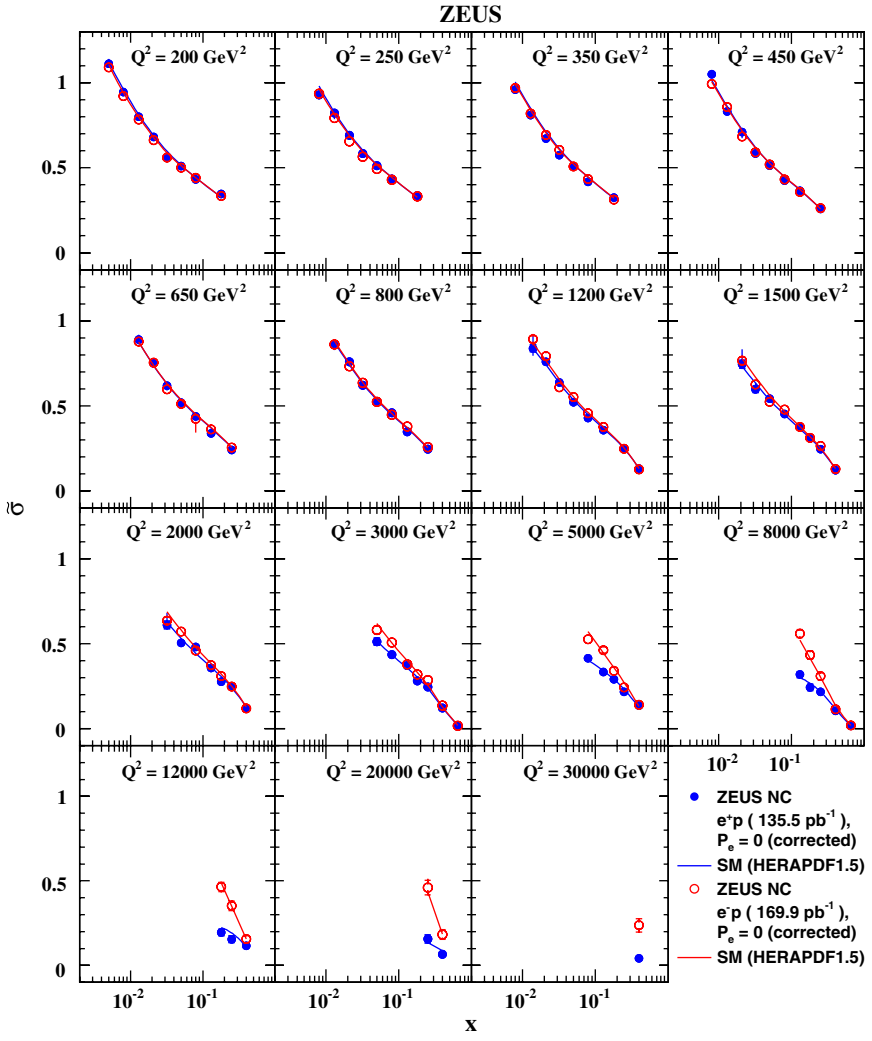

FIG. 5 (color online). The $e^{\pm}p$ unpolarized NC DIS reduced cross-section $\tilde{\sigma}$ plotted as a function of x at fixed Q^2. The closed (open) circles represent data points for e^+p (e^-p) collisions in which the inner error bars show the statistical uncertainty while the outer bars show the statistical and systematic uncertainties added in quadrature, although errors are too small to be seen in most cases. The curves show the predictions of the SM evaluated using the HERAPDF1.5 PDFs.

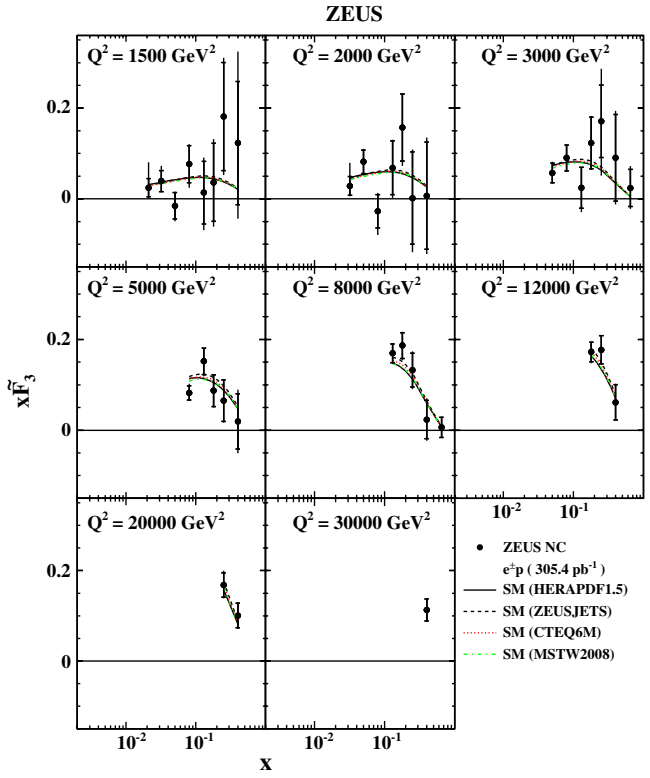

FIG. 6 (color online). The structure function $x\tilde{F}_3$ plotted as a function of x at fixed Q^2. The closed circles represent the ZEUS data. The inner error bars show the statistical uncertainty while the outer ones show the statistical and systematic uncertainties added in quadrature. The curves show the predictions of the SM evaluated using HERAPDF1.5 (solid), ZEUSJETS (dashed), CTEQ6M (dotted) and MSTW2008 (dash dotted) PDFs.

[36]. This was done by restricting the distance of closest approach between the track extrapolated to the calorimeter surface and the energy cluster position to within 10 cm and by requiring an electron track momentum (p_e^{trk}) larger than 3 GeV.
A matched track was not required if the electron emerged outside the acceptance of the tracking detectors.

(ii) Background rejection:
The requirement $38 < \delta < 65$ GeV was imposed to remove γp and beam-gas events and to reduce the number of events with significant QED initial-state radiation. To further reduce background from γp events, y_e was required to be less than 0.9. The measured P_T was expected to be small for NC events. Therefore, in order to remove cosmic rays and beam-related background events, the quantity $P_T/\sqrt{E_T}$ was required to be less than $4\sqrt{\mathrm{GeV}}$, and the quantity P_T/E_T was required to be less than 0.7.

(iii) Additional requirements:
The projection of γ_h onto the face of FCAL was required to be outside a radius of 18 cm centered on the beam-pipe axis, to reject events where most of the hadronic final state was lost in the forward beam pipe.
The Z coordinate of the ep interaction vertex reconstructed using tracks in the CTD and the MVD was required to satisfy $|Z_{\mathrm{vtx}}| < 30$ cm.
In order to avoid the kinematic region in which the MC simulation is not appropriate due to missing higher-order QED corrections [23], the requirement $y_{\mathrm{JB}}(1 - x_{\mathrm{DA}})^2 > 0.004$ was applied.
The final event sample was selected by requiring $Q^2_{\mathrm{DA}} > 185$ GeV^2.

A total of 302073 candidate events passed the selection criteria. The background contamination estimated from the γp MC was about 0.2% overall.

Figure 1 shows a comparison between data and MC distributions for the variables Q^2_{DA}, x_{DA}, y_{DA}, $E - P_Z$ of the event, θ_e and E'_e of the scattered electron and γ_h and $P_{T,h}$ of the final hadronic system. The description of the data by the MC is good.

VII. CROSS-SECTION DETERMINATION

The kinematic region of the measurement was defined as $Q^2 > 185$ GeV^2, $y < 0.9$ and $y(1 - x)^2 > 0.004$. The single-differential cross-sections $d\sigma/dQ^2$, $d\sigma/dx$ and $d\sigma/dy$ and the reduced cross-section $\tilde{\sigma}^{e^+p}$ were measured. In addition, the single-differential cross-sections $d\sigma/dx$ and $d\sigma/dy$ were measured for the restricted range $Q^2 > 3000$ GeV^2, $y < 0.9$ and $y(1 - x)^2 > 0.004$. The cross section in a particular bin ($d^2\sigma/dxdQ^2$ is used as an example) was determined according to

$$\frac{d^2\sigma}{dxdQ^2} = \frac{N_{\mathrm{data}} - N_{\mathrm{bg}}}{N_{\mathrm{MC}}} \cdot \frac{d^2\sigma^{\mathrm{SM}}_{\mathrm{Born}}}{dxdQ^2}, \tag{19}$$

where N_{data} is the number of data events in the bin, N_{bg} is the number of background events predicted from the photoproduction MC and N_{MC} is the number of signal MC events normalized to the luminosity of the data. The SM prediction for the Born-level cross section $d^2\sigma^{\mathrm{SM}}_{\mathrm{Born}}/dxdQ^2$ was evaluated using the CTEQ5D PDFs [24] as used for the MC simulation and using the PDG [37] values for the fine-structure constant, the mass of the Z boson and the weak mixing angle. This procedure implicitly takes into account the acceptance, bin centering and radiative corrections from the MC simulation. The bin sizes used for the determination of the single-differential and reduced cross sections were chosen to be commensurate with the detector resolutions. The statistical uncertainties on the cross sections were calculated from the number of events observed in the bins, taking into account the statistical uncertainty of the MC simulation (signal and background). Poisson statistics were used for all bins.

TABLE V. The structure-function $x\tilde{F}_3$ extracted using the e^+p data set ($\mathcal{L} = 135.5$ pb^{-1} corrected to $P_e = 0$) and previously published NC e^-p DIS results ($\mathcal{L} = 169.9$ pb^{-1} corrected to $P_e = 0$). The bin range and bin center for Q^2 and x, and measured $x\tilde{F}_3$ are shown.

Q^2 range (GeV^2)	Q_c^2 (GeV^2)	x range	x_c	$x\tilde{F}_3 \times 10$
1300–1800	1500	0.017–0.025	0.021	$0.24 \pm 0.20^{+0.53}_{-0.14}$
	1500	0.025–0.037	0.032	$0.39 \pm 0.23^{+0.24}_{-0.07}$
	1500	0.037–0.06	0.050	$-0.15 \pm 0.29^{+0.11}_{-0.15}$
	1500	0.06–0.1	0.080	$0.76 \pm 0.41^{+0.17}_{-0.16}$
	1500	0.1–0.15	0.130	$0.15 \pm 0.69^{+0.37}_{-0.32}$
	1500	0.15–0.23	0.180	$0.36 \pm 0.86^{+0.40}_{-0.33}$
	1500	0.23–0.35	0.250	$1.81 \pm 1.19^{+0.56}_{-0.43}$
	1500	0.35–0.53	0.400	$1.23 \pm 1.36^{+1.49}_{-0.92}$
1800–2500	2000	0.023–0.037	0.032	$0.29 \pm 0.21^{+0.45}_{-0.10}$
	2000	0.037–0.06	0.050	$0.81 \pm 0.26^{+0.12}_{-0.09}$
	2000	0.06–0.1	0.080	$-0.27 \pm 0.37^{+0.18}_{-0.19}$
	2000	0.1–0.15	0.130	$0.68 \pm 0.59^{+0.19}_{-0.16}$
	2000	0.15–0.23	0.180	$1.57 \pm 0.74^{+0.14}_{-0.33}$
	2000	0.23–0.35	0.250	$0.02 \pm 1.02^{+0.33}_{-0.42}$
	2000	0.35–0.53	0.400	$0.07 \pm 1.18^{+0.49}_{-0.51}$
2500–3500	3000	0.037–0.06	0.050	$0.57 \pm 0.21^{+0.12}_{-0.08}$
	3000	0.06–0.1	0.080	$0.90 \pm 0.29^{+0.09}_{-0.09}$
	3000	0.1–0.15	0.130	$0.24 \pm 0.45^{+0.16}_{-0.12}$
	3000	0.15–0.23	0.180	$1.23 \pm 0.57^{+0.22}_{-0.18}$
	3000	0.23–0.35	0.250	$1.71 \pm 0.80^{+0.84}_{-0.86}$
	3000	0.35–0.53	0.400	$0.90 \pm 0.96^{+0.40}_{-0.44}$
	3000	0.53–0.75	0.650	$0.24 \pm 0.41^{+0.26}_{-0.22}$
3500–5600	5000	0.04–0.1	0.080	$0.82 \pm 0.16^{+0.13}_{-0.05}$
	5000	0.1–0.15	0.130	$1.52 \pm 0.29^{+0.07}_{-0.07}$
	5000	0.15–0.23	0.180	$0.87 \pm 0.35^{+0.06}_{-0.11}$
	5000	0.23–0.35	0.250	$0.65 \pm 0.46^{+0.11}_{-0.09}$
	5000	0.35–0.53	0.400	$0.19 \pm 0.61^{+0.35}_{-0.35}$
5600–9000	8000	0.07–0.15	0.130	$1.70 \pm 0.21^{+0.09}_{-0.10}$
	8000	0.15–0.23	0.180	$1.87 \pm 0.29^{+0.11}_{-0.13}$
	8000	0.23–0.35	0.250	$1.33 \pm 0.37^{+0.17}_{-0.18}$
	8000	0.35–0.53	0.400	$0.24 \pm 0.42^{+0.20}_{-0.20}$
	8000	0.53–0.75	0.650	$0.06 \pm 0.22^{+0.08}_{-0.07}$
9000–15000	12000	0.09–0.23	0.180	$1.72 \pm 0.22^{+0.04}_{-0.12}$
	12000	0.23–0.35	0.250	$1.77 \pm 0.31^{+0.09}_{-0.09}$
	12000	0.35–0.53	0.400	$0.62 \pm 0.39^{+0.12}_{-0.11}$
15000–25000	20000	0.15–0.35	0.250	$1.68 \pm 0.27^{+0.17}_{-0.10}$
	20000	0.35–0.75	0.400	$1.01 \pm 0.28^{+0.09}_{-0.12}$
25000–50000	30000	0.25–0.75	0.400	$1.13 \pm 0.24^{+0.09}_{-0.09}$

TABLE VI. The interference structure-function $xF_3^{\gamma Z}$ evaluated at $Q^2 = 1500$ GeV^2 for x bins centered on x_c. The first (second) error on the measurement refers to the statistical (systematic) uncertainties.

Q^2 (GeV^2)	x_c	$xF_3^{\gamma Z} \times 10$
1500	0.021	$2.47 \pm 1.21^{+1.58}_{-0.82}$
	0.032	$1.16 \pm 1.05^{+1.31}_{-0.49}$
	0.050	$3.39 \pm 0.84^{+0.45}_{-0.35}$
	0.080	$3.19 \pm 0.52^{+0.37}_{-0.18}$
	0.130	$4.91 \pm 0.50^{+0.19}_{-0.20}$
	0.180	$4.51 \pm 0.41^{+0.11}_{-0.20}$
	0.250	$3.84 \pm 0.41^{+0.20}_{-0.15}$
	0.400	$2.16 \pm 0.35^{+0.12}_{-0.14}$
	0.650	$0.31 \pm 0.73^{+0.27}_{-0.24}$

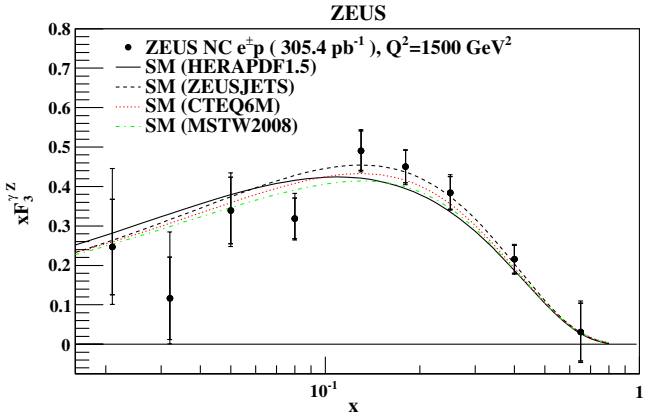

FIG. 7 (color online). The structure function $xF_3^{\gamma Z}$ extrapolated to a single Q^2 value of 1500 GeV^2 and plotted as a function of x. Other details as in Fig. 6.

VIII. SYSTEMATIC UNCERTAINTIES

Systematic uncertainties were estimated [30,36] by recalculating the cross sections after modifying the analysis, in turn, for the uncertainties detailed below.

(i) δ_1: The variation of the electron energy scale in the MC by its estimated uncertainty of $\pm 1\%$ resulted in changes of less than 0.5% in the cross sections over most of the kinematic region, due to the use of the DA reconstruction method. The effect was at most 3% in the high-y region of $d\sigma/dy$.

(ii) δ_2: The uncertainties due to "overlay" events, in which a DIS event overlapped with additional energy deposits from some other interaction in the RCAL were estimated by narrowing or widening the $38 < \delta < 65$ GeV interval symmetrically by ± 2 GeV.[4] The effect on the cross sections was typically below 1%. In a few high-Q^2 bins, the uncertainty was as large as 5%, reaching 11% in one reduced-cross-section bin.

(iii) δ_3: Systematic uncertainties arising from the normalization of the photoproduction background were determined by changing the background normalization by its estimated uncertainty of $\pm 50\%$ [38]. The resulting changes in the cross sections were typically below 0.5%, reaching about 2% in the medium-Q^2 reduced-cross-section bins.

(iv) δ_4: To estimate the systematic uncertainty associated with the electron finder, an alternative electron-finding algorithm [39] was used and the results were compared to those obtained using the nominal algorithm. The systematic uncertainty from the electron-finding procedure was below 1% for most of the phase space.

(v) δ_5: The upper limit of the θ range for which a matched track for the electron candidate was required was varied by ± 0.1 to account for uncertainties in the track-matching efficiency towards the edge of the CTD and BCAL. The uncertainty was mostly below 1.0%, but about 2% for the lower-Q^2 region.

(vi) δ_6: The systematic uncertainty due to the choice of the parton-shower scheme was evaluated by using the MEPS model of LEPTO to calculate the acceptance instead of ARIADNE.[5] The uncertainty was typically within 2%, but reached up to 5% in some bins of the reduced cross section and the highest bins of $d\sigma/dy$.

(vii) δ_7: The simulation of the first-level trigger was corrected in order to match the measured efficiency in the data. The systematic effect of the uncertainty of the correction on the cross section was typically less than 1%, but reached about 2% for medium Q^2 and high y.

(viii) δ_8: To evaluate the systematic uncertainty related to the electron isolation criterion, the isolation requirement was changed by ± 2 GeV from its nominal value of 5 GeV. The cross sections typically changed by much less than 0.5%.

(ix) δ_9: The distance of closest approach requirement was changed from 10 cm to 8 cm to estimate the uncertainty in the background contamination due to falsely identified electrons. The uncertainties in the cross sections associated with this variation were below 1% over most of the kinematic range.

[4]This would also affect remaining photoproduction events. However, their contribution was negligible.

[5]Since the simulation of the parton showers could, in principle, also have an influence on the electron isolation, the comparison was made removing the requirements on the electron isolation in order to prevent double counting of systematic uncertainty. However, no measurable influence of the isolation cut on δ_6 was observed.

TABLE VII. The reduced cross-section $\tilde{\sigma}$ for the reaction $e^+p \to e^+X$ ($\mathcal{L} = 78.8$ pb^{-1}, $P_e = +0.32$). The bin range, bin center (Q_c^2 and x_c) and measured cross section corrected to the electroweak Born level are shown. Other details as in Table I. This table has one continuation.

Q^2 range (GeV^2)	Q_c^2 (GeV^2)	x range	x_c	$\tilde{\sigma}$	N_{data}	$N_{\text{bg}}^{\text{MC}}$
185–240	200	0.004–0.006	0.005	$(1.125 \pm 0.013^{+0.026}_{-0.020})$	7884	66.0
	200	0.006–0.010	0.008	$(0.944 \pm 0.010^{+0.007}_{-0.016})$	9129	21.0
	200	0.010–0.017	0.013	$(0.797 \pm 0.008^{+0.003}_{-0.014})$	9345	7.4
	200	0.017–0.025	0.021	$(0.682 \pm 0.008^{+0.005}_{-0.005})$	6504	3.0
	200	0.025–0.037	0.032	$(0.563 \pm 0.007^{+0.014}_{-0.001})$	5678	0.0
	200	0.037–0.060	0.050	$(0.512 \pm 0.007^{+0.012}_{-0.003})$	6074	0.7
	200	0.060–0.120	0.080	$(0.434 \pm 0.005^{+0.013}_{-0.001})$	8126	0.0
	200	0.120–0.250	0.180	$(0.346 \pm 0.005^{+0.006}_{-0.004})$	5163	0.0
240–310	250	0.006–0.010	0.008	$(0.939 \pm 0.013^{+0.020}_{-0.006})$	5432	21.4
	250	0.010–0.017	0.013	$(0.822 \pm 0.010^{+0.007}_{-0.013})$	6209	6.3
	250	0.017–0.025	0.021	$(0.710 \pm 0.010^{+0.003}_{-0.011})$	4663	5.0
	250	0.025–0.037	0.032	$(0.606 \pm 0.009^{+0.011}_{-0.012})$	4518	0.7
	250	0.037–0.060	0.050	$(0.514 \pm 0.008^{+0.014}_{-0.008})$	4529	0.0
	250	0.060–0.120	0.080	$(0.437 \pm 0.006^{+0.009}_{-0.005})$	5960	0.0
	250	0.120–0.250	0.180	$(0.340 \pm 0.005^{+0.006}_{-0.009})$	4741	0.0
310–410	350	0.006–0.010	0.008	$(0.962 \pm 0.017^{+0.020}_{-0.007})$	3313	16.5
	350	0.010–0.017	0.013	$(0.817 \pm 0.013^{+0.011}_{-0.004})$	4131	4.0
	350	0.017–0.025	0.021	$(0.689 \pm 0.012^{+0.010}_{-0.004})$	3088	0.0
	350	0.025–0.037	0.032	$(0.576 \pm 0.011^{+0.017}_{-0.003})$	2847	0.7
	350	0.037–0.060	0.050	$(0.520 \pm 0.009^{+0.010}_{-0.007})$	3181	0.7
	350	0.060–0.120	0.080	$(0.426 \pm 0.007^{+0.014}_{-0.005})$	4063	0.0
	350	0.120–0.250	0.180	$(0.336 \pm 0.005^{+0.006}_{-0.005})$	3834	0.0
410–530	450	0.006–0.010	0.008	$(1.044 \pm 0.020^{+0.020}_{-0.014})$	2718	26.7
	450	0.010–0.017	0.013	$(0.828 \pm 0.019^{+0.013}_{-0.007})$	1957	4.5
	450	0.017–0.025	0.021	$(0.715 \pm 0.018^{+0.014}_{-0.005})$	1607	1.3
	450	0.025–0.037	0.032	$(0.598 \pm 0.014^{+0.011}_{-0.004})$	1779	0.6
	450	0.037–0.060	0.050	$(0.504 \pm 0.011^{+0.009}_{-0.005})$	2087	0.0
	450	0.060–0.100	0.080	$(0.434 \pm 0.010^{+0.009}_{-0.003})$	1968	0.0
	450	0.100–0.170	0.130	$(0.382 \pm 0.009^{+0.009}_{-0.001})$	1891	0.0
	450	0.170–0.300	0.250	$(0.264 \pm 0.007^{+0.006}_{-0.001})$	1571	0.0
530–710	650	0.010–0.017	0.013	$(0.899 \pm 0.018^{+0.019}_{-0.014})$	2458	16.6
	650	0.017–0.025	0.021	$(0.763 \pm 0.019^{+0.007}_{-0.007})$	1551	0.0
	650	0.025–0.037	0.032	$(0.627 \pm 0.018^{+0.015}_{-0.005})$	1222	0.7
	650	0.037–0.060	0.050	$(0.520 \pm 0.015^{+0.003}_{-0.004})$	1199	0.0
	650	0.060–0.100	0.080	$(0.440 \pm 0.013^{+0.004}_{-0.003})$	1071	0.0
	650	0.100–0.170	0.130	$(0.320 \pm 0.011^{+0.010}_{-0.001})$	892	0.0
	650	0.170–0.300	0.250	$(0.244 \pm 0.008^{+0.004}_{-0.003})$	869	0.0
710–900	800	0.009–0.017	0.013	$(0.874 \pm 0.022^{+0.022}_{-0.013})$	1590	24.4
	800	0.017–0.025	0.021	$(0.748 \pm 0.023^{+0.008}_{-0.008})$	1039	1.9
	800	0.025–0.037	0.032	$(0.605 \pm 0.019^{+0.006}_{-0.006})$	1014	4.6
	800	0.037–0.060	0.050	$(0.534 \pm 0.015^{+0.010}_{-0.003})$	1192	0.7
	800	0.060–0.100	0.080	$(0.455 \pm 0.014^{+0.003}_{-0.005})$	1031	0.0
	800	0.100–0.170	0.130	$(0.363 \pm 0.012^{+0.008}_{-0.002})$	850	0.0
	800	0.170–0.300	0.250	$(0.243 \pm 0.010^{+0.007}_{-0.003})$	646	0.0

TABLE VII. (*Continued*)

Q^2 range (GeV^2)	Q_c^2 (GeV^2)	x range	x_c	$\tilde{\sigma}$	N_{data}	$N_{\text{bg}}^{\text{MC}}$
900–1300	1200	0.010–0.017	0.014	$(0.854 \pm 0.028^{+0.065}_{-0.026})$	994	20.9
	1200	0.017–0.025	0.021	$(0.758 \pm 0.023^{+0.017}_{-0.009})$	1090	7.1
	1200	0.025–0.037	0.032	$(0.641 \pm 0.019^{+0.006}_{-0.008})$	1114	0.0
	1200	0.037–0.060	0.050	$(0.531 \pm 0.015^{+0.009}_{-0.004})$	1334	0.0
	1200	0.060–0.100	0.080	$(0.437 \pm 0.012^{+0.005}_{-0.003})$	1227	0.7
	1200	0.100–0.170	0.130	$(0.365 \pm 0.011^{+0.004}_{-0.003})$	1115	0.0
	1200	0.170–0.300	0.250	$(0.259 \pm 0.009^{+0.002}_{-0.002})$	893	0.0
	1200	0.300–0.530	0.400	$(0.133 \pm 0.007^{+0.002}_{-0.001})$	375	0.0
1300–1800	1500	0.017–0.025	0.021	$(0.747 \pm 0.032^{+0.088}_{-0.013})$	556	10.5
	1500	0.025–0.037	0.032	$(0.585 \pm 0.025^{+0.040}_{-0.005})$	558	1.2
	1500	0.037–0.060	0.050	$(0.562 \pm 0.020^{+0.005}_{-0.011})$	806	0.6
	1500	0.060–0.100	0.080	$(0.458 \pm 0.016^{+0.006}_{-0.004})$	780	0.0
	1500	0.100–0.150	0.130	$(0.387 \pm 0.017^{+0.004}_{-0.005})$	547	0.7
	1500	0.150–0.230	0.180	$(0.329 \pm 0.015^{+0.003}_{-0.003})$	496	0.0
	1500	0.230–0.350	0.250	$(0.249 \pm 0.014^{+0.005}_{-0.002})$	318	0.0
	1500	0.350–0.530	0.400	$(0.115 \pm 0.010^{+0.002}_{-0.004})$	142	0.0
1800–2500	2000	0.023–0.037	0.032	$(0.584 \pm 0.030^{+0.080}_{-0.011})$	402	7.1
	2000	0.037–0.060	0.050	$(0.523 \pm 0.024^{+0.005}_{-0.008})$	486	0.7
	2000	0.060–0.100	0.080	$(0.503 \pm 0.021^{+0.004}_{-0.005})$	582	0.7
	2000	0.100–0.150	0.130	$(0.355 \pm 0.019^{+0.003}_{-0.004})$	358	0.7
	2000	0.150–0.230	0.180	$(0.275 \pm 0.016^{+0.001}_{-0.006})$	294	0.0
	2000	0.230–0.350	0.250	$(0.254 \pm 0.017^{+0.004}_{-0.007})$	233	0.0
	2000	0.350–0.530	0.400	$(0.120 \pm 0.012^{+0.007}_{-0.001})$	106	0.0
2500–3500	3000	0.037–0.060	0.050	$(0.497 \pm 0.029^{+0.013}_{-0.011})$	290	1.3
	3000	0.060–0.100	0.080	$(0.434 \pm 0.024^{+0.009}_{-0.005})$	338	0.0
	3000	0.100–0.150	0.130	$(0.380 \pm 0.023^{+0.007}_{-0.006})$	271	0.0
	3000	0.150–0.230	0.180	$(0.300 \pm 0.020^{+0.007}_{-0.004})$	225	0.0
	3000	0.230–0.350	0.250	$(0.264 \pm 0.020^{+0.002}_{-0.004})$	181	0.0
	3000	0.350–0.530	0.400	$(0.114 \pm 0.014^{+0.003}_{-0.005})$	70	0.0
	3000	0.530–0.750	0.650	$(0.016^{+0.006\ +0.002}_{-0.004\ -0.000})$	13	0.0
3500–5600	5000	0.040–0.100	0.080	$(0.450 \pm 0.023^{+0.017}_{-0.006})$	401	2.3
	5000	0.100–0.150	0.130	$(0.370 \pm 0.025^{+0.007}_{-0.006})$	224	0.0
	5000	0.150–0.230	0.180	$(0.326 \pm 0.022^{+0.002}_{-0.008})$	220	0.0
	5000	0.230–0.350	0.250	$(0.235 \pm 0.019^{+0.002}_{-0.005})$	147	0.0
	5000	0.350–0.530	0.400	$(0.149 \pm 0.016^{+0.003}_{-0.002})$	88	0.0
5600–9000	8000	0.070–0.150	0.130	$(0.339 \pm 0.026^{+0.011}_{-0.016})$	173	0.0
	8000	0.150–0.230	0.180	$(0.229 \pm 0.024^{+0.003}_{-0.005})$	89	0.0
	8000	0.230–0.350	0.250	$(0.241 \pm 0.026^{+0.004}_{-0.007})$	89	0.0
	8000	0.350–0.530	0.400	$(0.111^{+0.020\ +0.006}_{-0.017\ -0.003})$	41	0.0
	8000	0.530–0.750	0.650	$(0.020^{+0.008\ +0.002}_{-0.006\ -0.002})$	10	0.0
9000–15000	12000	0.090–0.230	0.180	$(0.218 \pm 0.028^{+0.007}_{-0.012})$	62	0.0
	12000	0.230–0.350	0.250	$(0.188^{+0.035\ +0.004}_{-0.030\ -0.013})$	40	0.0
	12000	0.350–0.530	0.400	$(0.148^{+0.030\ +0.003}_{-0.026\ -0.007})$	33	0.0
15000–25000	20000	0.150–0.350	0.250	$(0.135^{+0.039\ +0.020}_{-0.031\ -0.003})$	19	0.0
	20000	0.350–0.750	0.400	$(0.059^{+0.029\ +0.006}_{-0.020\ -0.008})$	8	0.0
25000–50000	30000	0.250–0.750	0.400	$(0.023^{+0.031\ +0.001}_{-0.015\ -0.022})$	2	0.0

TABLE VIII. The reduced cross-section $\tilde{\sigma}$ for the reaction $e^+p \to e^+X$ ($\mathcal{L} = 56.7$ pb^{-1}, $P_e = -0.36$). The bin range, bin center (Q_c^2 and x_c) and measured cross section corrected to the electroweak Born level are shown. Other details as in Table I. This table has one continuation.

Q^2 range (GeV^2)	Q_c^2 (GeV^2)	x range	x_c	$\tilde{\sigma}$	N_{data}	$N_{\text{bg}}^{\text{MC}}$
185–240	200	0.004–0.006	0.005	$(1.090 \pm 0.015^{+0.025}_{-0.020})$	5429	43.9
	200	0.006–0.010	0.008	$(0.947 \pm 0.012^{+0.009}_{-0.023})$	6518	15.4
	200	0.010–0.017	0.013	$(0.807 \pm 0.010^{+0.003}_{-0.015})$	6729	6.3
	200	0.017–0.025	0.021	$(0.679 \pm 0.010^{+0.005}_{-0.005})$	4603	2.1
	200	0.025–0.037	0.032	$(0.571 \pm 0.009^{+0.015}_{-0.003})$	4089	0.0
	200	0.037–0.060	0.050	$(0.510 \pm 0.008^{+0.011}_{-0.002})$	4301	0.5
	200	0.060–0.120	0.080	$(0.431 \pm 0.006^{+0.012}_{-0.001})$	5741	0.0
	200	0.120–0.250	0.180	$(0.346 \pm 0.006^{+0.006}_{-0.005})$	3660	0.0
240–310	250	0.006–0.010	0.008	$(0.916 \pm 0.015^{+0.026}_{-0.009})$	3758	14.3
	250	0.010–0.017	0.013	$(0.821 \pm 0.012^{+0.005}_{-0.013})$	4402	4.0
	250	0.017–0.025	0.021	$(0.667 \pm 0.012^{+0.008}_{-0.005})$	3107	3.4
	250	0.025–0.037	0.032	$(0.557 \pm 0.010^{+0.010}_{-0.009})$	2948	0.5
	250	0.037–0.060	0.050	$(0.513 \pm 0.009^{+0.014}_{-0.009})$	3211	0.0
	250	0.060–0.120	0.080	$(0.432 \pm 0.007^{+0.009}_{-0.004})$	4182	0.0
	250	0.120–0.250	0.180	$(0.334 \pm 0.006^{+0.004}_{-0.007})$	3301	0.0
310–410	350	0.006–0.010	0.008	$(0.929 \pm 0.020^{+0.031}_{-0.011})$	2266	10.3
	350	0.010–0.017	0.013	$(0.799 \pm 0.015^{+0.009}_{-0.005})$	2869	3.9
	350	0.017–0.025	0.021	$(0.652 \pm 0.014^{+0.010}_{-0.003})$	2079	0.4
	350	0.025–0.037	0.032	$(0.576 \pm 0.013^{+0.012}_{-0.006})$	2022	0.4
	350	0.037–0.060	0.050	$(0.489 \pm 0.011^{+0.010}_{-0.004})$	2125	0.5
	350	0.060–0.120	0.080	$(0.407 \pm 0.008^{+0.014}_{-0.003})$	2760	0.0
	350	0.120–0.250	0.180	$(0.310 \pm 0.006^{+0.005}_{-0.003})$	2506	0.0
410–530	450	0.006–0.010	0.008	$(0.997 \pm 0.024^{+0.021}_{-0.021})$	1830	19.0
	450	0.010–0.017	0.013	$(0.802 \pm 0.022^{+0.010}_{-0.013})$	1347	2.8
	450	0.017–0.025	0.021	$(0.696 \pm 0.021^{+0.010}_{-0.005})$	1104	0.9
	450	0.025–0.037	0.032	$(0.563 \pm 0.016^{+0.011}_{-0.006})$	1183	0.5
	450	0.037–0.060	0.050	$(0.523 \pm 0.013^{+0.013}_{-0.001})$	1531	0.0
	450	0.060–0.100	0.080	$(0.415 \pm 0.011^{+0.007}_{-0.005})$	1337	0.0
	450	0.100–0.170	0.130	$(0.342 \pm 0.010^{+0.010}_{-0.001})$	1203	0.0
	450	0.170–0.300	0.250	$(0.248 \pm 0.008^{+0.009}_{-0.001})$	1041	0.0
530–710	650	0.010–0.017	0.013	$(0.821 \pm 0.021^{+0.033}_{-0.017})$	1587	12.1
	650	0.017–0.025	0.021	$(0.699 \pm 0.022^{+0.010}_{-0.011})$	1013	0.0
	650	0.025–0.037	0.032	$(0.587 \pm 0.020^{+0.015}_{-0.006})$	821	0.5
	650	0.037–0.060	0.050	$(0.503 \pm 0.017^{+0.004}_{-0.005})$	829	0.0
	650	0.060–0.100	0.080	$(0.426 \pm 0.016^{+0.002}_{-0.006})$	738	0.0
	650	0.100–0.170	0.130	$(0.358 \pm 0.013^{+0.009}_{-0.001})$	706	0.0
	650	0.170–0.300	0.250	$(0.232 \pm 0.010^{+0.003}_{-0.002})$	584	0.0
710–900	800	0.009–0.017	0.013	$(0.786 \pm 0.025^{+0.036}_{-0.015})$	1010	17.3
	800	0.017–0.025	0.021	$(0.734 \pm 0.027^{+0.012}_{-0.014})$	718	1.4
	800	0.025–0.037	0.032	$(0.620 \pm 0.023^{+0.012}_{-0.008})$	733	3.3
	800	0.037–0.060	0.050	$(0.489 \pm 0.018^{+0.012}_{-0.007})$	774	0.2
	800	0.060–0.100	0.080	$(0.456 \pm 0.017^{+0.005}_{-0.005})$	737	0.0
	800	0.100–0.170	0.130	$(0.320 \pm 0.014^{+0.006}_{-0.003})$	537	0.0
	800	0.170–0.300	0.250	$(0.244 \pm 0.011^{+0.008}_{-0.003})$	464	0.0

TABLE VIII. (*Continued*)

Q^2 range (GeV^2)	Q_c^2 (GeV^2)	x range	x_c	$\tilde{\sigma}$	N_{data}	$N_{\text{bg}}^{\text{MC}}$
900–1300	1200	0.010–0.017	0.014	$(0.769 \pm 0.031^{+0.085}_{-0.025})$	637	14.9
	1200	0.017–0.025	0.021	$(0.715 \pm 0.027^{+0.019}_{-0.014})$	729	4.9
	1200	0.025–0.037	0.032	$(0.608 \pm 0.022^{+0.011}_{-0.010})$	749	0.0
	1200	0.037–0.060	0.050	$(0.490 \pm 0.017^{+0.007}_{-0.006})$	875	0.0
	1200	0.060–0.100	0.080	$(0.406 \pm 0.014^{+0.006}_{-0.004})$	810	0.5
	1200	0.100–0.170	0.130	$(0.336 \pm 0.012^{+0.003}_{-0.003})$	730	0.0
	1200	0.170–0.300	0.250	$(0.232 \pm 0.010^{+0.002}_{-0.002})$	566	0.0
	1200	0.300–0.530	0.400	$(0.125 \pm 0.008^{+0.002}_{-0.003})$	249	0.0
1300–1800	1500	0.017–0.025	0.021	$(0.699 \pm 0.037^{+0.083}_{-0.020})$	368	7.1
	1500	0.025–0.037	0.032	$(0.585 \pm 0.030^{+0.011}_{-0.011})$	394	0.7
	1500	0.037–0.060	0.050	$(0.496 \pm 0.022^{+0.007}_{-0.009})$	503	0.5
	1500	0.060–0.100	0.080	$(0.434 \pm 0.019^{+0.005}_{-0.005})$	523	0.0
	1500	0.100–0.150	0.130	$(0.356 \pm 0.019^{+0.005}_{-0.004})$	355	0.3
	1500	0.150–0.230	0.180	$(0.276 \pm 0.016^{+0.004}_{-0.002})$	293	0.0
	1500	0.230–0.350	0.250	$(0.234 \pm 0.016^{+0.006}_{-0.003})$	210	0.0
	1500	0.350–0.530	0.400	$(0.126 \pm 0.012^{+0.004}_{-0.004})$	109	0.0
1800–2500	2000	0.023–0.037	0.032	$(0.615 \pm 0.036^{+0.044}_{-0.015})$	299	5.1
	2000	0.037–0.060	0.050	$(0.464 \pm 0.027^{+0.029}_{-0.007})$	304	0.5
	2000	0.060–0.100	0.080	$(0.439 \pm 0.023^{+0.006}_{-0.007})$	358	0.4
	2000	0.100–0.150	0.130	$(0.351 \pm 0.022^{+0.011}_{-0.004})$	249	0.4
	2000	0.150–0.230	0.180	$(0.273 \pm 0.019^{+0.006}_{-0.004})$	205	0.0
	2000	0.230–0.350	0.250	$(0.239 \pm 0.019^{+0.005}_{-0.006})$	154	0.0
	2000	0.350–0.530	0.400	$(0.120 \pm 0.014^{+0.002}_{-0.004})$	74	0.0
2500–3500	3000	0.037–0.060	0.050	$(0.511 \pm 0.035^{+0.012}_{-0.012})$	212	0.8
	3000	0.060–0.100	0.080	$(0.429 \pm 0.028^{+0.006}_{-0.013})$	237	0.0
	3000	0.100–0.150	0.130	$(0.350 \pm 0.026^{+0.008}_{-0.007})$	177	0.0
	3000	0.150–0.230	0.180	$(0.247 \pm 0.022^{+0.007}_{-0.008})$	131	0.0
	3000	0.230–0.350	0.250	$(0.217 \pm 0.021^{+0.003}_{-0.011})$	105	0.0
	3000	0.350–0.530	0.400	$(0.133 \pm 0.018^{+0.006}_{-0.005})$	57	0.0
	3000	0.530–0.750	0.650	$(0.014^{+0.007\ +0.001}_{-0.005\ -0.000})$	8	0.0
3500–5600	5000	0.040–0.100	0.080	$(0.351 \pm 0.023^{+0.016}_{-0.010})$	227	1.7
	5000	0.100–0.150	0.130	$(0.276 \pm 0.025^{+0.005}_{-0.010})$	120	0.0
	5000	0.150–0.230	0.180	$(0.235 \pm 0.022^{+0.003}_{-0.006})$	113	0.0
	5000	0.230–0.350	0.250	$(0.191 \pm 0.021^{+0.004}_{-0.003})$	85	0.0
	5000	0.350–0.530	0.400	$(0.118 \pm 0.017^{+0.002}_{-0.003})$	49	0.0
5600–9000	8000	0.070–0.150	0.130	$(0.281 \pm 0.028^{+0.013}_{-0.007})$	104	0.0
	8000	0.150–0.230	0.180	$(0.258 \pm 0.030^{+0.003}_{-0.014})$	72	0.0
	8000	0.230–0.350	0.250	$(0.179 \pm 0.026^{+0.006}_{-0.003})$	47	0.0
	8000	0.350–0.530	0.400	$(0.096^{+0.023\ +0.002}_{-0.019\ -0.006})$	25	0.0
	8000	0.530–0.750	0.650	$(0.014^{+0.010\ +0.003}_{-0.006\ -0.003})$	5	0.0
9000–15000	12000	0.090–0.230	0.180	$(0.161^{+0.033\ +0.012}_{-0.028\ -0.006})$	33	0.0
	12000	0.230–0.350	0.250	$(0.106^{+0.034\ +0.002}_{-0.026\ -0.003})$	16	0.0
	12000	0.350–0.530	0.400	$(0.070^{+0.028\ +0.008}_{-0.021\ -0.006})$	11	0.0
15000–25000	20000	0.150–0.350	0.250	$(0.185^{+0.053\ +0.017}_{-0.042\ -0.018})$	19	0.0
	20000	0.350–0.750	0.400	$(0.073^{+0.040\ +0.009}_{-0.027\ -0.026})$	7	0.0
25000–50000	30000	0.250–0.750	0.400	$(0.065^{+0.052\ +0.026}_{-0.031\ -0.005})$	4	0.0

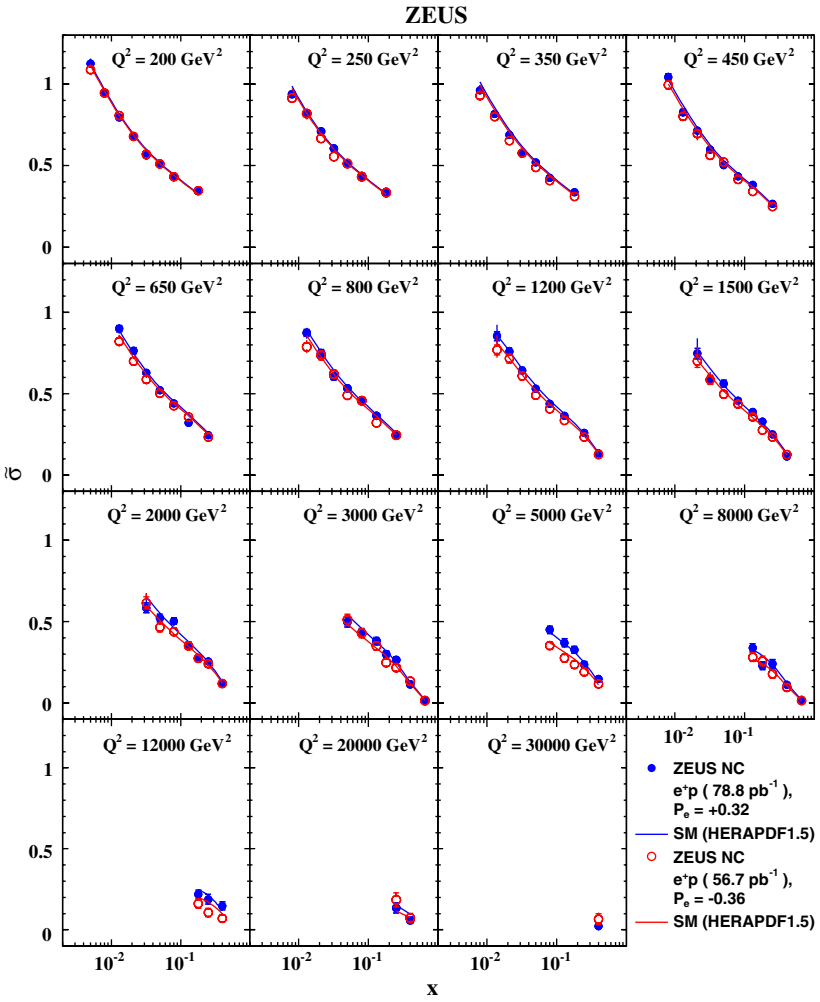

FIG. 8 (color online). The e^+p NC DIS reduced cross-section $\tilde{\sigma}$ for positively and negatively polarized beams plotted as a function of x at fixed Q^2. The closed (open) circles represent the ZEUS data for negative (positive) polarization. Other details as in Fig. 5.

(x) δ_{10}: The energy resolution used in the MC for the scattered electron was varied by its estimated uncertainty $\pm 1\%$. The effect on the cross sections was mostly less than 0.5% and less than 1% over the full kinematic range.

(xi) δ_{11}: To account for differences of the p_e^{trk} distributions in data and MC, the p_e^{trk} requirement was varied by ± 1 GeV, resulting in a variation of the cross section by less than 0.5% over most of the kinematic range, and up to 6% in a few reduced-cross-section bins.

(xii) δ_{12}: The cut of 18 cm on the projected radius of the hadronic angle onto the FCAL was varied by ± 2 cm. The cross sections typically changed by much less than 0.5%. The effect rises up to a maximum of 7% for the highest bins of both $d\sigma/dy$ and the reduced cross section.

(xiii) δ_{13}: The variation of the hadronic energy scale by its estimated uncertainty of $\pm 2\%$ in the MC resulted in changes of mostly below 0.5% and always less than 2% in the cross sections over the full kinematic range.

(xiv) δ_{14}: The systematic uncertainty associated with cosmic-ray rejection was evaluated by varying the $P_T/\sqrt{E_T}$ cut by $\pm 1\sqrt{\mathrm{GeV}}$ and the P_T/E_T cut by ± 0.1. The cross section uncertainties were mostly below 0.5% reaching a maximum of 6% in one reduced-cross-section bin for the variation of the $p_T/\sqrt{E_T}$ cut.

(xv) δ_{15}: The limit on the accepted $|Z_{\mathrm{vtx}}|$ was varied by ± 5 cm, resulting in less than a 1% change in the cross sections over most of the kinematic range, reaching a maximum of 6% in the highest-Q^2 bins.

The 15 sources of systematic uncertainty were treated as uncorrelated to each other. Bin-to-bin correlations were found for δ 1,2,3,4,6,8,10,12 and 13. The positive and negative deviations from the nominal cross section values were added in quadrature separately to obtain the total positive and negative systematic uncertainty.

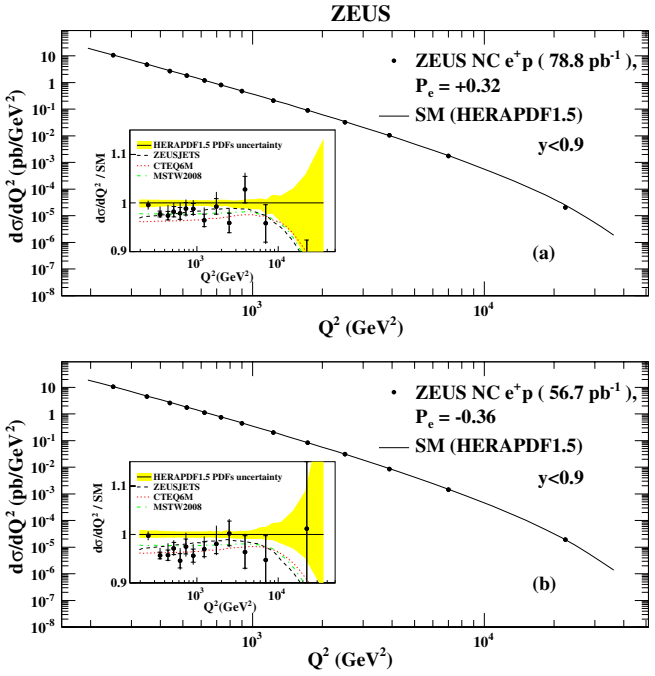

FIG. 9 (color online). The e^+p NC DIS cross-section $d\sigma/dQ^2$ for $y < 0.9$ and $y(1-x)^2 > 0.004$ for (a) positive and (b) negative polarization. Other details as in Fig. 2.

The relative uncertainty in the measured polarization was 4%. This has a negligible effect on the cross sections. The choice of which polarimeter to consider was made run by run to maximize the available luminosity and minimize the uncertainty in the measured polarization.

The measured luminosity had a relative uncertainty of 1.8% for the period with right-handed polarization and 1.9% for the period with left-handed polarization. The uncertainties in the luminosity and polarization measurements were not included in the total systematic uncertainty shown in the final results.

IX. RESULTS

A. Unpolarized cross sections

The single-differential cross sections as a function of Q^2, x and y extracted using the full data sample are shown in Figs. 2–4 and tabulated in Tables I, II, and III. In all tables, the total systematic uncertainty as described in Sec. VIII is given. The numbers for the individual contributions are available electronically [40,41].

Combining the data from the negatively and positively polarized beams resulted in a residual polarization of 0.03 which was corrected for using theoretical predictions in NLO QCD with electroweak corrections.

The measurement of $d\sigma/dQ^2$ shown in Fig. 2 falls over 7 orders of magnitude in the measured range covering 2 orders of magnitude in Q^2. In this figure, the ratio of the measured cross sections and the SM predictions evaluated using the HERAPDF1.5 PDFs [42,43] and the PDFs from ZEUSJETS [44], CTEQ6M [45] and MSTW2008 [46] are shown.

The SM predictions differ depending on the PDFs. Taking into account the luminosity uncertainty, which is not shown in the figures, the data are well described by the SM predictions. The cross sections $d\sigma/dx$ and $d\sigma/dy$ are

TABLE IX. The single-differential cross-section $d\sigma/dQ^2$ [$y < 0.9$, $y(1-x)^2 > 0.004$] for the reaction $e^+p \to e^+X$ ($\mathcal{L} = 78.8$ pb^{-1} $P_e = +0.32$). The bin range, bin center (Q_c^2) and measured cross section corrected to the electroweak Born level are shown. Other details as in Table I.

Q^2 range (GeV^2)	Q_c^2 (GeV^2)	$d\sigma/dQ^2$ (pb/GeV^2)	N_{data}	$N_{\text{bg}}^{\text{MC}}$
185–300	250	$(1.07 \pm 0.00^{+0.01}_{-0.01}) \times 10^{1}$	96158	155.9
300–400	350	$(4.74 \pm 0.03^{+0.07}_{-0.03})$	28667	37.0
400–475	440	$(2.72 \pm 0.03^{+0.06}_{-0.01})$	11858	39.1
475–565	520	$(1.83 \pm 0.02^{+0.03}_{-0.01})$	8698	23.4
565–672	620	$(1.19 \pm 0.02^{+0.02}_{-0.01})$	6108	24.1
672–800	730	$(8.01 \pm 0.11^{+0.11}_{-0.07}) \times 10^{-1}$	5859	22.3
800–1050	900	$(4.75 \pm 0.05^{+0.07}_{-0.04}) \times 10^{-1}$	7622	28.9
1050–1460	1230	$(2.11 \pm 0.03^{+0.05}_{-0.02}) \times 10^{-1}$	5875	32.9
1460–2080	1730	$(9.00 \pm 0.15^{+0.23}_{-0.07}) \times 10^{-2}$	3832	15.6
2080–3120	2500	$(3.28 \pm 0.07^{+0.07}_{-0.02}) \times 10^{-2}$	2298	6.1
3120–5220	3900	$(1.04 \pm 0.03^{+0.02}_{-0.01}) \times 10^{-2}$	1416	2.9
5220–12500	7000	$(1.73 \pm 0.07^{+0.02}_{-0.03}) \times 10^{-3}$	616	0.0
12500–51200	22400	$(2.03 \pm 0.26^{+0.02}_{-0.06}) \times 10^{-5}$	60	0.0

TABLE X. The single-differential cross-section $d\sigma/dx$ [$y < 0.9$, $y(1-x)^2 > 0.004$] for $Q^2 > 185$ GeV^2 and $Q^2 > 3000$ GeV^2 for the reaction $e^+p \to e^+X$ ($\mathcal{L} = 78.8$ pb^{-1}, $P_e = +0.32$). The Q^2 and bin range, bin center (x_c) and measured cross section corrected to the electroweak Born level are shown. Other details as in Table I.

$Q^2>$ (GeV^2)	x range	x_c	$d\sigma/dx$ (pb)	N_{data}	$N_{\text{bg}}^{\text{MC}}$
185	$(0.63-1.00)\times10^{-2}$	0.794×10^{-2}	$(8.80\pm0.06^{+0.12}_{-0.08})\times10^4$	20397	96.7
	$(0.10-0.16)\times10^{-1}$	0.126×10^{-1}	$(5.88\pm0.04^{+0.06}_{-0.07})\times10^4$	23452	72.3
	$(0.16-0.25)\times10^{-1}$	0.200×10^{-1}	$(3.69\pm0.02^{+0.03}_{-0.03})\times10^4$	23332	51.2
	$(0.25-0.40)\times10^{-1}$	0.316×10^{-1}	$(2.12\pm0.01^{+0.04}_{-0.01})\times10^4$	22669	17.5
	$(0.40-0.63)\times10^{-1}$	0.501×10^{-1}	$(1.25\pm0.01^{+0.02}_{-0.01})\times10^4$	19901	3.3
	$(0.63-1.00)\times10^{-1}$	0.794×10^{-1}	$(6.98\pm0.05^{+0.11}_{-0.03})\times10^3$	18738	2.9
	0.10–0.16	0.126	$(3.97\pm0.03^{+0.06}_{-0.02})\times10^3$	18025	1.3
	0.16–0.25	0.200	$(2.09\pm0.02^{+0.04}_{-0.03})\times10^3$	11263	0.0
3000	$(0.40-0.63)\times10^{-1}$	0.501×10^{-1}	$(1.81\pm0.11^{+0.08}_{-0.03})\times10^2$	269	0.6
	$(0.63-1.00)\times10^{-1}$	0.794×10^{-1}	$(1.69\pm0.08^{+0.04}_{-0.02})\times10^2$	437	2.3
	0.10–0.16	0.126	$(1.28\pm0.06^{+0.01}_{-0.02})\times10^2$	542	0.0
	0.16–0.25	0.200	$(7.46\pm0.34^{+0.07}_{-0.12})\times10^1$	471	0.0
	0.25–0.40	0.316	$(3.41\pm0.18^{+0.08}_{-0.03})\times10^1$	350	0.0
	0.40–0.75	0.687	$(1.29\pm0.11^{+0.03}_{-0.03})$	151	0.0

shown in Figs. 3 and 4 for the nominal range $Q^2 > 185$ GeV^2 and for $Q^2 > 3000$ GeV^2. The figures demonstrate the precision of this measurement. The measured cross sections are well described by the SM prediction evaluated using the HERAPDF1.5 PDFs.[6]

The reduced cross sections of unpolarized e^+p NC DIS tabulated in Table IV are shown in Fig. 5. The residual polarization was corrected for using theoretical predictions. The SM predictions are in good agreement with the measurements over the full kinematic range. Also shown are the unpolarized e^-p NC DIS cross sections measured using an integrated luminosity of 169.9 pb^{-1} collected between 2005 and 2006 [5]. In Sec. II, it was discussed that the e^-p and e^+p reduced cross sections only differ at high Q^2. As the contribution of $x\tilde{F}_3$ has to be extracted through a subtraction [see Eq. (4)], a very precise measurement of these cross sections is needed.

Figure 6 shows the result on $x\tilde{F}_3$ obtained according to Eq. (4) from the unpolarized e^+p and e^-p reduced cross sections in the high-Q^2 region. The systematic uncertainties were treated as uncorrelated between the e^+p and the e^-p measurements in the extraction of $x\tilde{F}_3$. The measurements are well described by the SM predictions. The results are also given in Table V.

The structure function $xF_3^{\gamma Z}$ has little dependence on Q^2. Therefore a higher statistical significance could be obtained by averaging the measurements after an extrapolation to 1500 GeV^2. The structure function $xF_3^{\gamma Z}$ measured at $Q^2 = 1500$ GeV^2, tabulated in Table VI, is shown in Fig. 7. It is well described by the SM predictions.

The inclusive cross sections presented here provide valuable information to the global fits [46,47] for parton distribution functions over a wide range of Bjorken x values from $\sim10^{-2}$ to 0.65.

B. Polarized cross sections

The effects of the longitudinal polarization of the electrons becomes significant at the electroweak scale, where the contributions of both γ and Z exchange to the cross section are comparable. The reduced cross sections for positive and negative longitudinal polarizations tabulated in Tables VII and VIII are shown in Fig. 8. The data are also well described by the SM predictions using the HERAPDF1.5 PDFs. At high Q^2, a difference between the positively and negatively polarized cross sections is predicted. To demonstrate this effect, the single-differential cross section $d\sigma/dQ^2$ was measured separately for positive and negative beam polarizations. The results are shown in Fig. 9. Both measurements are well described by the SM predictions using different sets of PDFs taking the uncertainty due to the luminosity measurement into account. The single-differential cross sections as a function of Q^2, x and y extracted using the negatively and positively polarized data samples separately are tabulated in Tables IX, X, XI, XII, XIII, and XIV.

The ratio of the measured single-differential cross section $d\sigma/dQ^2$ for the two different polarization states is shown in Fig. 10(a). The difference between the two polarization states is clearly visible at higher Q^2. The

[6]HERAPDF1.5 is based on HERA I and HERA II data, but the data presented here are not used for the extraction.

TABLE XI. The single-differential cross-section $d\sigma/dy$ for $Q^2 > 185$ GeV^2 and $Q^2 > 3000$ GeV^2 $[y(1-x)^2 > 0.004]$ for the reaction $e^+p \to e^+X$ ($\mathcal{L} = 78.8$ pb^{-1}, $P_e = +0.32$). The Q^2 and bin range, bin center (y_c) and measured cross section corrected to the electroweak Born level are shown. Other details as in Table I.

$Q^2>$ (GeV^2)	y range	y_c	$d\sigma/dy$ (pb)	N_{data}	$N_{\text{bg}}^{\text{MC}}$
185	0.00–0.05	0.025	$(1.65 \pm 0.01^{+0.03}_{-0.01}) \times 10^4$	44541	0.0
	0.05–0.10	0.075	$(8.19 \pm 0.05^{+0.15}_{-0.05}) \times 10^3$	29853	4.4
	0.10–0.15	0.125	$(5.73 \pm 0.04^{+0.04}_{-0.05}) \times 10^3$	20723	9.0
	0.15–0.20	0.175	$(4.41 \pm 0.04^{+0.02}_{-0.05}) \times 10^3$	15423	13.7
	0.20–0.25	0.225	$(3.66 \pm 0.03^{+0.02}_{-0.04}) \times 10^3$	12419	11.1
	0.25–0.30	0.275	$(2.96 \pm 0.03^{+0.03}_{-0.02}) \times 10^3$	9588	10.2
	0.30–0.35	0.325	$(2.58 \pm 0.03^{+0.04}_{-0.02}) \times 10^3$	8283	25.8
	0.35–0.40	0.375	$(2.25 \pm 0.03^{+0.04}_{-0.03}) \times 10^3$	7167	29.1
	0.40–0.45	0.425	$(2.01 \pm 0.03^{+0.03}_{-0.02}) \times 10^3$	6164	38.0
	0.45–0.50	0.475	$(1.76 \pm 0.02^{+0.05}_{-0.02}) \times 10^3$	5223	29.4
	0.50–0.55	0.525	$(1.56 \pm 0.02^{+0.04}_{-0.01}) \times 10^3$	4534	32.9
	0.55–0.60	0.575	$(1.46 \pm 0.02^{+0.04}_{-0.02}) \times 10^3$	4079	36.4
	0.60–0.65	0.625	$(1.31 \pm 0.02^{+0.03}_{-0.02}) \times 10^3$	3415	35.5
	0.65–0.70	0.675	$(1.22 \pm 0.02^{+0.05}_{-0.03}) \times 10^3$	2788	14.6
	0.70–0.75	0.725	$(1.13 \pm 0.02^{+0.07}_{-0.03}) \times 10^3$	2097	28.9
	0.75–0.90	0.825	$(9.73 \pm 0.19^{+0.73}_{-0.27}) \times 10^2$	2685	66.9
3000	0.05–0.10	0.075	$(3.50 \pm 0.34^{+0.05}_{-0.07}) \times 10^1$	109	0.0
	0.10–0.15	0.125	$(5.86 \pm 0.41^{+0.08}_{-0.06}) \times 10^1$	201	0.0
	0.15–0.20	0.175	$(6.38 \pm 0.43^{+0.04}_{-0.13}) \times 10^1$	225	0.0
	0.20–0.25	0.225	$(6.32 \pm 0.42^{+0.08}_{-0.08}) \times 10^1$	226	0.0
	0.25–0.30	0.275	$(5.59 \pm 0.39^{+0.03}_{-0.12}) \times 10^1$	204	0.0
	0.30–0.35	0.325	$(5.66 \pm 0.40^{+0.05}_{-0.07}) \times 10^1$	206	0.0
	0.35–0.40	0.375	$(3.90 \pm 0.33^{+0.07}_{-0.07}) \times 10^1$	142	0.0
	0.40–0.45	0.425	$(3.56 \pm 0.31^{+0.05}_{-0.05}) \times 10^1$	130	0.0
	0.45–0.50	0.475	$(3.62 \pm 0.32^{+0.14}_{-0.09}) \times 10^1$	131	0.0
	0.50–0.55	0.525	$(2.89 \pm 0.29^{+0.03}_{-0.14}) \times 10^1$	103	0.0
	0.55–0.60	0.575	$(3.19 \pm 0.30^{+0.23}_{-0.03}) \times 10^1$	112	0.0
	0.60–0.65	0.625	$(2.55 \pm 0.26^{+0.15}_{-0.04}) \times 10^1$	93	2.3
	0.65–0.70	0.675	$(2.69 \pm 0.28^{+0.06}_{-0.13}) \times 10^1$	92	0.0
	0.70–0.75	0.725	$(2.39 \pm 0.27^{+0.07}_{-0.16}) \times 10^1$	79	0.0
	0.75–0.80	0.775	$(2.17 \pm 0.26^{+0.10}_{-0.07}) \times 10^1$	71	0.0
	0.80–0.85	0.825	$(2.16 \pm 0.26^{+0.28}_{-0.06}) \times 10^1$	68	0.6
	0.85–0.90	0.875	$(1.98 \pm 0.28^{+0.15}_{-0.20}) \times 10^1$	52	0.0

asymmetry A^+ [see Eq. (13)] extracted from these measurements is tabulated in Table XV and is shown in Fig. 10(b), where only statistical uncertainties are considered. The uncertainty in A^+ arising from the relative normalization between the data sets was evaluated to be 1%. The other systematic uncertainties are assumed to cancel. The SM also describes these results well. The deviation of A^+ from zero, particularly at high Q^2, shows the difference in the behavior of the two polarization states and is clear evidence of parity violation. The precision of

TABLE XII. The single-differential cross-section $d\sigma/dQ^2$ [$y < 0.9$, $y(1-x)^2 > 0.004$] for the reaction $e^+p \to e^+X$ ($\mathcal{L} = 56.7$ pb^{-1} $P_e = -0.36$). The bin range, bin center (Q_c^2) and measured cross section corrected to the electroweak Born level are shown. Other details as in Table I.

Q^2 range (GeV^2)	Q_c^2 (GeV^2)	$d\sigma/dQ^2$ (pb/GeV^2)	N_{data}	$N_{\text{bg}}^{\text{MC}}$
185–300	250	$(1.06 \pm 0.00^{+0.01}_{-0.01}) \times 10^1$	67629	108.0
300–400	350	$(4.56 \pm 0.03^{+0.07}_{-0.03})$	19579	22.7
400–475	440	$(2.62 \pm 0.03^{+0.06}_{-0.02})$	8079	25.8
475–565	520	$(1.77 \pm 0.02^{+0.02}_{-0.02})$	5919	16.1
565–672	620	$(1.11 \pm 0.02^{+0.03}_{-0.01})$	4058	16.6
672–800	730	$(7.64 \pm 0.12^{+0.19}_{-0.11}) \times 10^{-1}$	3969	15.2
800–1050	900	$(4.41 \pm 0.06^{+0.09}_{-0.06}) \times 10^{-1}$	4994	20.4
1050–1460	1230	$(2.01 \pm 0.03^{+0.04}_{-0.02}) \times 10^{-1}$	3948	22.1
1460–2080	1730	$(8.26 \pm 0.17^{+0.27}_{-0.10}) \times 10^{-2}$	2485	10.5
2080–3120	2500	$(3.11 \pm 0.08^{+0.05}_{-0.04}) \times 10^{-2}$	1541	4.1
3120–5220	3900	$(8.54 \pm 0.30^{+0.15}_{-0.11}) \times 10^{-3}$	826	2.3
5220–12500	7000	$(1.43 \pm 0.08^{+0.02}_{-0.02}) \times 10^{-3}$	361	0.0
12500–51200	22400	$(1.93^{+0.35+0.11}_{-0.30-0.14}) \times 10^{-5}$	41	0.0

TABLE XIII. The single-differential cross-section $d\sigma/dx$ [$y < 0.9$, $y(1-x)^2 > 0.004$] for $Q^2 > 185$ GeV^2 and $Q^2 > 3000$ GeV^2 for the reaction $e^+p \to e^+X$ ($\mathcal{L} = 56.7$ pb^{-1}, $P_e = -0.36$). The Q^2 and bin range, bin center (x_c) and measured cross section corrected to the electroweak Born level are shown. Other details as in Table I.

$Q^2>$ (GeV^2)	x range	x_c	$d\sigma/dx$ (pb)	N_{data}	$N_{\text{bg}}^{\text{MC}}$
185	$(0.63-1.00) \times 10^{-2}$	0.794×10^{-2}	$(8.61 \pm 0.07^{+0.16}_{-0.13}) \times 10^4$	14173	67.6
	$(0.10-0.16) \times 10^{-1}$	0.126×10^{-1}	$(5.79 \pm 0.05^{+0.07}_{-0.07}) \times 10^4$	16410	52.4
	$(0.16-0.25) \times 10^{-1}$	0.200×10^{-1}	$(3.54 \pm 0.03^{+0.03}_{-0.02}) \times 10^4$	15901	34.2
	$(0.25-0.40) \times 10^{-1}$	0.316×10^{-1}	$(2.07 \pm 0.02^{+0.03}_{-0.01}) \times 10^4$	15715	12.1
	$(0.40-0.63) \times 10^{-1}$	0.501×10^{-1}	$(1.21 \pm 0.01^{+0.02}_{-0.01}) \times 10^4$	13656	2.2
	$(0.63-1.00) \times 10^{-1}$	0.794×10^{-1}	$(6.84 \pm 0.06^{+0.11}_{-0.03}) \times 10^3$	13087	2.1
	0.10–0.16	0.126	$(3.79 \pm 0.03^{+0.05}_{-0.01}) \times 10^3$	12219	0.7
	0.16–0.25	0.200	$(1.97 \pm 0.02^{+0.03}_{-0.04}) \times 10^3$	7505	0.0
3000	$(0.40-0.63) \times 10^{-1}$	0.501×10^{-1}	$(1.61 \pm 0.12^{+0.05}_{-0.04}) \times 10^2$	171	0.7
	$(0.63-1.00) \times 10^{-1}$	0.794×10^{-1}	$(1.50 \pm 0.09^{+0.05}_{-0.02}) \times 10^2$	277	1.7
	0.l0–0.16	0.126	$(1.05 \pm 0.06^{+0.01}_{-0.04}) \times 10^2$	317	0.0
	0.16–0.25	0.200	$(5.81 \pm 0.36^{+0.11}_{-0.10}) \times 10^1$	259	0.0
	0.25–0.40	0.316	$(3.02 \pm 0.21^{+0.04}_{-0.05}) \times 10^1$	217	0.0
	0.40–0.75	0.687	$(1.10 \pm 0.12^{+0.04}_{-0.03})$	89	0.0

the data makes the effect also clearly visible at relatively low Q^2, where it is intrinsically small.

The effect of γ/Z interference is quantified by calculating the χ^2 per degree of freedom (DOF) of A^+ with respect both to zero and to the SM prediction using the HERAPDF1.5 PDFs. The χ^2/DOF with respect to zero is determined to be 9.0, whereas the χ^2/DOF with respect to the SM prediction is 1.5. Thus parity violation in ep NC DIS is demonstrated at scales down to $\approx 10^{-18}$ m.

TABLE XIV. The single-differential cross-section $d\sigma/dy$ for $Q^2 > 185$ GeV^2 and $Q^2 > 3000$ GeV^2 $[y(1-x)^2 > 0.004]$ for the reaction $e^+p \to e^+X$ ($\mathcal{L} = 56.7$ pb^{-1}, $P_e = -0.36$). The Q^2 and bin range, bin center (y_c) and measured cross section corrected to the electroweak Born level are shown. Other details as in Table I.

$Q^2>$ (GeV^2)	y range	y_c	$d\sigma/dy$ (pb)	N_{data}	$N_{\text{bg}}^{\text{MC}}$
185	0.00–0.05	0.025	$(1.60 \pm 0.01^{+0.02}_{-0.01}) \times 10^4$	30773	0.0
	0.05–0.10	0.075	$(7.98 \pm 0.06^{+0.14}_{-0.04}) \times 10^3$	20679	3.0
	0.10–0.15	0.125	$(5.53 \pm 0.05^{+0.03}_{-0.04}) \times 10^3$	14221	6.0
	0.15–0.20	0.175	$(4.34 \pm 0.04^{+0.03}_{-0.06}) \times 10^3$	10814	10.0
	0.20–0.25	0.225	$(3.55 \pm 0.04^{+0.03}_{-0.04}) \times 10^3$	8555	8.1
	0.25–0.30	0.275	$(2.89 \pm 0.04^{+0.05}_{-0.05}) \times 10^3$	6666	8.3
	0.30–0.35	0.325	$(2.47 \pm 0.03^{+0.04}_{-0.03}) \times 10^3$	5636	18.0
	0.35–0.40	0.375	$(2.24 \pm 0.03^{+0.01}_{-0.03}) \times 10^3$	5035	19.1
	0.40–0.45	0.425	$(1.95 \pm 0.03^{+0.04}_{-0.02}) \times 10^3$	4238	25.7
	0.45–0.50	0.475	$(1.68 \pm 0.03^{+0.05}_{-0.02}) \times 10^3$	3538	19.1
	0.50–0.55	0.525	$(1.52 \pm 0.03^{+0.04}_{-0.02}) \times 10^3$	3127	22.8
	0.55–0.60	0.575	$(1.38 \pm 0.03^{+0.04}_{-0.02}) \times 10^3$	2715	24.9
	0.60–0.65	0.625	$(1.26 \pm 0.03^{+0.06}_{-0.03}) \times 10^3$	2308	25.8
	0.65–0.70	0.675	$(1.18 \pm 0.03^{+0.03}_{-0.04}) \times 10^3$	1883	10.3
	0.70–0.75	0.725	$(1.11 \pm 0.03^{+0.07}_{-0.04}) \times 10^3$	1445	18.9
	0.75–0.90	0.825	$(9.26 \pm 0.22^{+0.84}_{-0.36}) \times 10^2$	1748	42.2
3000	0.05–0.10	0.075	$(2.99 \pm 0.37^{+0.09}_{-0.06}) \times 10^1$	65	0.0
	0.10–0.15	0.125	$(5.21 \pm 0.47^{+0.05}_{-0.09}) \times 10^1$	125	0.0
	0.15–0.20	0.175	$(5.33 \pm 0.46^{+0.15}_{-0.07}) \times 10^1$	132	0.0
	0.20–0.25	0.225	$(4.73 \pm 0.43^{+0.09}_{-0.20}) \times 10^1$	119	0.0
	0.25–0.30	0.275	$(4.19 \pm 0.40^{+0.06}_{-0.06}) \times 10^1$	108	0.0
	0.30–0.35	0.325	$(4.47 \pm 0.42^{+0.07}_{-0.08}) \times 10^1$	115	0.0
	0.35–0.40	0.375	$(3.54 \pm 0.37^{+0.06}_{-0.12}) \times 10^1$	91	0.0
	0.40–0.45	0.425	$(3.24 \pm 0.35^{+0.04}_{-0.18}) \times 10^1$	84	0.0
	0.45–0.50	0.475	$(3.61 \pm 0.37^{+0.06}_{-0.24}) \times 10^1$	93	0.0
	0.50–0.55	0.525	$(2.77 \pm 0.33^{+0.06}_{-0.07}) \times 10^1$	70	0.0
	0.55–0.60	0.575	$(2.64 \pm 0.33^{+0.31}_{-0.06}) \times 10^1$	66	0.0
	0.60–0.65	0.625	$(2.26 \pm 0.29^{+0.17}_{-0.06}) \times 10^1$	59	1.7
	0.65–0.70	0.675	$(1.72^{+0.31+0.08}_{-0.27-0.07}) \times 10^1$	42	0.0
	0.70–0.75	0.725	$(2.32 \pm 0.31^{+0.05}_{-0.07}) \times 10^1$	55	0.0
	0.75–0.80	0.775	$(2.05 \pm 0.30^{+0.20}_{-0.09}) \times 10^1$	48	0.2
	0.80–0.85	0.825	$(1.55^{+0.31+0.27}_{-0.26-0.07}) \times 10^1$	35	0.5
	0.85–0.90	0.875	$(1.87^{+0.37+0.12}_{-0.32-0.12}) \times 10^1$	35	0.0

The polarized cross sections presented here constrain the vector couplings of the quarks to the Z [see Eq. (15)] when included in the PDF fits. Therefore, this measurement is a stringent test of the electroweak sector of the Standard Model. The data can also be used to test physics beyond the Standard Model like setting limits on the production of leptoquarks [48].

X. CONCLUSIONS

The cross sections for neutral current deep inelastic e^+p scattering with a longitudinally polarized positron beam have been measured. The measurements were based on a data sample corresponding to an integrated luminosity of 135.5 pb^{-1} collected with the ZEUS detector at HERA

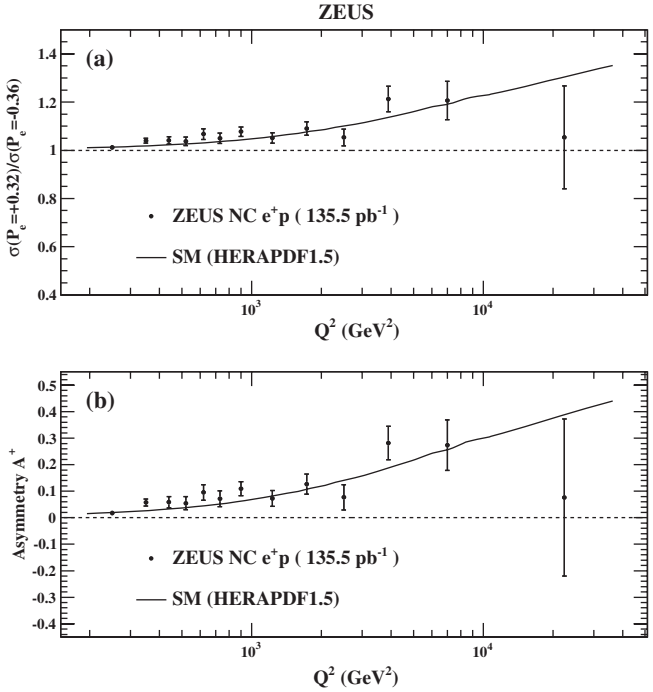

FIG. 10. The (a) ratio of $d\sigma/dQ^2$ using positive and negative polarization and (b) the polarization asymmetry A^+ as functions of Q^2. The closed circles represent ZEUS data. Only statistical uncertainties are considered as the systematic uncertainties are assumed to cancel. The curves show the predictions of the SM evaluated using the HERAPDF1.5 PDFs.

from 2006 to 2007 at a center-of-mass energy of 318 GeV. The accessible range in Q^2 extended to $Q^2 = 50000$ GeV^2 allowing for a stringent test of electroweak effects in the Standard Model.

The single-differenteial cross sections as a function of Q^2, x and y were presented for $Q^2 > 185$ GeV^2, $y < 0.9$ and $y(1-x)^2 > 0.004$, where the data obtained with negatively and positively polarized beams were combined. The cross sections $d\sigma/dx$ and $d\sigma/dy$ were also measured for $Q^2 > 3000$ GeV^2, $y < 0.9$ and $y(1-x)^2 > 0.004$. The reduced cross section was measured at zero polarization by correcting for the residual polarization of the combined data sample. These measurements were combined with previously measured $e^- p$ neutral current cross sections to extract $x\tilde{F}_3$. In addition, the interference structure function $xF_3^{\gamma Z}$ was extracted at an average value of $Q^2 = 1500$ GeV^2.

The reduced cross section and the single-differential cross sections $d\sigma/dQ^2$, $d\sigma/dx$ and $d\sigma/dy$ were also measured separately for positive and negative values of the longitudinal polarization of the positron beam. Parity violation was observed through the polarization asymmetry A^+. The measured cross sections confirmed the predictions of the Standard Model and provided strong constraints at the electroweak scale.

ACKNOWLEDGMENTS

We appreciate the contributions to the construction and maintenance of the ZEUS detector of many people who are not listed as authors. The HERA machine group and the DESY computing staff are especially acknowledged for their success in providing excellent operation of the collider and the data-analysis environment. We thank the DESY directorate for their strong support and encouragement. C. G. is an STFC Advanced Fellow. This material was based on work supported by the National Science Foundation, while J. J. W. worked at the foundation.

TABLE XV. The polarization asymmetry measured using positively and negatively polarized $e^+ p$ beams ($\mathcal{L} = 78.8$ pb^{-1} $P_e = +0.32$ and $\mathcal{L} = 56.7$ pb^{-1} $P_e = -0.36$, respectively). The bin range, bin center (Q_c^2), the cross section ratio of the samples with $P_e = +0.32$ and $P_e = -0.36$ and the measured asymmetry A^+ are shown. Only the statistical uncertainties on the measurement are shown as systematic uncertainties are assumed to cancel.

Q^2 range (GeV^2)	Q_c^2 (GeV^2)	Ratio	Asymmetry A^+ $\times 10$
185.0–300.0	250	1.01 ± 0.01	0.17 ± 0.07
300.0–400.0	350	1.04 ± 0.01	0.57 ± 0.14
400.0–475.7	440	1.04 ± 0.02	0.58 ± 0.21
475.7–565.7	520	1.04 ± 0.02	0.55 ± 0.25
565.7–672.7	620	1.07 ± 0.02	0.95 ± 0.30
672.7–800.0	730	1.05 ± 0.02	0.71 ± 0.30
800.0–1050.0	900	1.08 ± 0.02	1.10 ± 0.27
1050.0–1460.0	1230	1.05 ± 0.02	0.73 ± 0.30
1460.0–2080.0	1730	1.09 ± 0.03	1.26 ± 0.38
2080.0–3120.0	2500	1.05 ± 0.03	0.77 ± 0.48
3120.0–5220.0	3900	1.21 ± 0.05	2.82 ± 0.63
5220.0–12500.0	7000	1.21 ± 0.08	2.74 ± 0.95
12500.0–51200.0	22400	1.05 ± 0.21	0.76 ± 2.96

Support was provided by the following: U.S. Department of Energy; Italian National Institute for Nuclear Physics (INFN); German Federal Ministry for Education and Research (BMBF) under Contract No. 05 H09PDF; the Science and Technology Facilities Council, UK; a F. R. S. grant from the Malaysian government; the U.S. National Science Foundation (any opinions, findings and conclusions or recommendations expressed in this material are those of the authors and do not necessarily reflect the views of the National Science Foundation); the Polish Ministry of Science and Higher Education as a scientific Project No. DPN/N188/DESY/2009; the Polish Ministry of Science and Higher Education and its grants for scientific research; the German Federal Ministry for Education and Research (BMBF) under Contract No. 05h09GUF, and the SFB 676 of the Deutsche Forschungsgemeinschaft (DFG); the Japanese Ministry of Education, Culture, Sports, Science and Technology (MEXT) and its grants for scientific research; the Korean Ministry of Education and Korea Science and Engineering Foundation; the FNRS and its associated funds (IISN and FRIA) and by an Inter-University Attraction Poles Programme subsidized by the Belgian Federal Science Policy Office; the Spanish Ministry of Education and Science through funds provided by CICYT; the Natural Sciences and Engineering Research Council of Canada (NSERC); the German Federal Ministry for Education and Research (BMBF); R. F. Presidential Grant No. N 4142.2010.2 for Leading Scientific Schools, by the Russian Ministry of Education and Science through its grant for Scientific Research on High Energy Physics and under Contract No. 02.740.11.0244; the Netherlands Foundation for Research on Matter (FOM); the Israel Science Foundation, Max Planck Institute for Physics, Munich, Germany; the Polish National Science Centre, Project No. DEC-2011/01/BST2/03643; Warsaw University, Poland; DESY, Germany; and Russian Foundation for Basic Research, Grant No. 11-02-91345-DFG_a.

[1] H. Abramowicz and A. Caldwell, Rev. Mod. Phys. **71**, 1275 (1999).
[2] F. D. Aaron *et al.* (H1 Collaboration and ZEUS Collaboration), J. High Energy Phys. 01 (2010) 109.
[3] S. Chekanov *et al.* (ZEUS Collaboration), Phys. Lett. B **637**, 210 (2006).
[4] S. Chekanov *et al.* (ZEUS Collaboration), Eur. Phys. J. C **61**, 223 (2009).
[5] S. Chekanov *et al.* (ZEUS Collaboration), Eur. Phys. J. C **62**, 625 (2009).
[6] S. Chekanov *et al.* (ZEUS Collaboration), Eur. Phys. J. C **70**, 945 (2010).
[7] A. Aktas *et al.* (H1 Collaboration), J. High Energy Phys. 09 (2012) 061.
[8] R. Devenish and A. Cooper-Sarkar, *Deep Inelastic Scattering* (Oxford University, New York, 2003).
[9] M. Klein and T. Riemann, Z. Phys. C **24**, 151 (1984).
[10] S. Chekanov *et al.* (ZEUS Collaboration), Phys. Lett. B **682**, 8 (2009).
[11] A. Aktas *et al.* (H1 Collaboration), Eur. Phys. J. C **71**, 1579 (2011).
[12] Zeus Collaboration, The ZEUS Detector Status Report 1993, http://www-zeus.desy.de/bluebook/bluebook.html.
[13] N. Harnew, G. P. Heath, M. D. Jeffs, J. Nash, G. L. Salmon, P. D. Shield, D. J. White, and F. F. Wilson, Nucl. Instrum. Methods Phys. Res., Sect. A **279**, 290 (1989); B. Foster *et al.*, Nucl. Phys. B, Proc. Suppl. **32**, 181 (1993); Nucl. Instrum. Methods Phys. Res., Sect. A **338**, 254 (1994).
[14] A. Polini *et al.*, Nucl. Instrum. Methods Phys. Res., Sect. A **581**, 656 (2007).
[15] M. Derrick, D. Gacek, N. Hill, B. Musgrave, R. Noland, E. Petereit, J. Repond, R. Stanek, and K. Sugano, Nucl. Instrum. Methods Phys. Res., Sect. A **309**, 77 (1991); A. Andresen *et al.*, Nucl. Instrum. Methods Phys. Res., Sect. A **309**, 101 (1991); A. Caldwell *et al.*, Nucl. Instrum. Methods Phys. Res., Sect. A **321**, 356 (1992); A. Bernstein *et al.*, Nucl. Instrum. Methods Phys. Res., Sect. A **336**, 23 (1993).
[16] J. Andruszków *et al.*, DESY Report No. DESY-92-066, 1992; M. Derrick *et al.* (ZEUS Collaboration), Z. Phys. C **63**, 391 (1994); J. Andruszków *et al.*, Acta Phys. Pol. B **32**, 2025 (2001).
[17] M. Helbich, Y. Ning, S. Paganis, Z. Ren, W. B. Schmidke, F. Sciulli, U. Schneekloth, C. Büttner, A. Caldwell, and J. Sutiak, Nucl. Instrum. Methods Phys. Res., Sect. A **565**, 572 (2006).
[18] A. A. Sokolov and I. M. Ternov, Sov. Phys. Dokl. **8**, 1203 (1964).
[19] V. N. Baier and V. A. Khoze, Sov. J. Nucl. Phys. **9**, 238 (1969).
[20] D. P. Barber *et al.*, Nucl. Instrum. Methods Phys. Res., Sect. A **329**, 79 (1993).
[21] M. Beckmann *et al.*, Nucl. Instrum. Methods Phys. Res., Sect. A **479**, 334 (2002).
[22] A. Kwiatkowski, H. Spiesberger, and H.-J. Möhring, Comput. Phys. Commun. **69**, 155 (1992); *Proceedings of Workshop on Physics at HERA*, edited by W. Buchmüller and G. Ingelman (DESY, Hamburg, 1991).
[23] G. A. Schuler and H. Spiesberger, *Proceedings of Workshop on Physics at HERA*, edited by W. Buchmüller and G. Ingelman (DESY, Hamburg, 1991), Vol. 3, p. 1419; H. Spiesberger, HERACLES and DJANGOH: Event Generation for ep Interactions at HERA Including Radiative Processes, http://www.desy.de/~hspiesb/djangoh.html.

[24] H. L. Lai, J. Huston, S. Kuhlmann, J. Morfin, F. Olness, J. F. Owens, J. Pumplin, and W. K. Tung (CTEQ Collabotation), Eur. Phys. J. C **12**, 375 (2000).
[25] L. Lönnblad, Comput. Phys. Commun. **71**, 15 (1992).
[26] A. Edin, G. Ingelman, and J. Rathsman, Phys. Lett. B **366**, 371 (1996).
[27] T. Sjöstrand, Comput. Phys. Commun. **39**, 347 (1986); T. Sjöstrand and M. Bengtsson, Comput. Phys. Commun. **43**, 367 (1987); T. Sjöstrand, Comput. Phys. Commun. **82**, 74 (1994).
[28] G. Marchesini, B. R. Webber, G. Abbiendi, I. G. Knowles, M. H. Seymour, and L. Stanco, Comput. Phys. Commun. **67**, 465 (1992).
[29] R. Brun *et al.*, CERN Report No. CERN-DD/EE/84-1, 1987 (unpublished).
[30] T. Stewart, Ph.D. Thesis, University of Toronto, 2012.
[31] S. Bentvelsen, J. Engelen, and P. Kooijman, *Proceedings of Workshop on Physics at HERA*, edited by W. Buchmüller and G. Ingelman (DESY, Hamburg, 1992), Vol. 1, p. 23.
[32] K. C. Höger, *Proceedings of Workshop on Physics at HERA*, edited by W. Buchmüller and G. Ingelman (DESY, Hamburg, 1992), Vol. 1, p. 43.
[33] F. Jacquet and A. Blondel, *Proceedings of the Study for an ep Facility for Europe*, edited by U. Amaldi (DESY, Hamburg, 1979), p. 391; W. H. Smith, K. Tokushuku, and L. W. Wiggers, in *Proceedings of Computing in High-Energy Physics (CHEP), Annecy, France, 1992*, edited by C. Verkerk and W. Wojcik (CERN, Geneva, 1992), p. 222.
[34] P. D. Allfrey *et al.*, Nucl. Instrum. Methods Phys. Res., Sect. A **580**, 1257 (2007).
[35] J. Breitweg *et al.* (ZEUS Collaboration), Eur. Phys. J. C **11**, 427 (1999).
[36] F. Januschek, Ph.D. Thesis, University of Hamburg, 2012.
[37] D. E. Groom *et al.* (Particle Data Group), Eur. Phys. J. C **15**, 1 (2000).
[38] M. Wlasenko, Ph.D. Thesis, University of Bonn, 2009.
[39] H. Abramowicz, A. Caldwell, and R. Sinkus, Nucl. Instrum. Methods Phys. Res., Sect. A **365**, 508 (1995).
[40] ZEUS Collaboration, ZEUS database, http://www-zeus.desy.de/zeus_papers/zeus_papers.html#12-145.
[41] Durham University, The Durham HepData Project, http://hepdata.cedar.ac.uk/.
[42] H. Abramowicz *et al.* (H1 Collaboration and ZEUS Collaboration), Reports No. H1prelim-10-142 and No. ZEUS-prel-10-018, https://www.desy.de/h1zeus/combined_results/herapdftable/.
[43] V. Radescu, in *Proceedings of the 35th International Conference on High Energy Physics, ICHEP 2010, Paris, France, 2010*, edited by B. Pire (POS, SISSA, Italy, 2010), p. 168.
[44] S. Chekanov *et al.* (ZEUS Collaboration), Eur. Phys. J. C **42**, 1 (2005).
[45] J. Pumplin, D. R. Stump, J. Huston, H.-L. Lai, P. Nadolsky, and W.-K. Tung, J. High Energy Phys. 07 (2002) 012.
[46] A. D. Martin, W. J. Stirling, R. S. Thorne, and G. Watt, Eur. Phys. J. C **63**, 189 (2009).
[47] P. M. Nadolsky, H.-L. Lai, Q.-H. Cao, J. Huston, J. Pumplin, D. Stump, W.-K. Tung, and C.-P. Yuan, Phys. Rev. D **78**, 013004 (2008).
[48] H. Abramovic *et al.* (ZEUS Collaboration), Phys. Rev. D **86**, 012005 (2012).